Hindawi
Mathematical Problems in Engineering
Volume 2022, Article ID 4756347, 24 pages
https://doi.org/10.1155/2022/4756347

Research Article

Maiden Application of a Modified HBA-Optimized Cascaded (2DOF + FOPIDN)-PD Controller for Load Frequency Control of Diverse Source Power System

Stephen Oladipo[1], **Yanxia Sun**[1] and **Zenghui Wang**[2]

[1]*Department of Electrical and Electronic Engineering Science, University of Johannesburg, Johannesburg 2006, South Africa*
[2]*Department of Electrical Engineering, University of South Africa, Johannesburg 1710, South Africa*

Correspondence should be addressed to Yanxia Sun; sunyanxia@gmail.com

Received 17 May 2022; Revised 6 September 2022; Accepted 29 October 2022; Published 15 November 2022

Academic Editor: Wesley Peres

Electricity has become one of the most essential components of establishing a quality standard of living in any country. Consequently, considerable work has been focused on designing a sophisticated load frequency control (LFC) system. However, in light of limited resources and real-world challenges, computationally based control algorithms that are more effective and less expensive remain critically needed. Thus, this paper employs a modified honey badger algorithm (HBA) in conjunction with the concepts of Lévy flight and inertia weight to optimize the parameters of a new cascaded two-degree-of-freedom fractional-PID structure coupled with a proportional derivative (2DOF + FOPIDN)-PD controller to solve LFC problems in an interconnected power system (IPS) comprising conventional and renewable energy sources (RES). The proposed control technique is applied to a two-area IPS under diverse load conditions and in the presence of nonlinear elements and electronic devices. The proposed method is evaluated with respect to a range of performance metrics, such as settling time, undershoots, and error criteria values. The collective performance of the established control scheme indicated that the suggested control approach provides excellent reliability under various load condition scenarios, sensitivity tests, and perturbations, proving the system's efficacy and dependability.

1. Introduction

1.1. Literature Review. The fundamental task of electric utility companies is to guarantee an uninterrupted supply of electricity to consumers through the process of generation, transmission, and distribution. A proportional active power generation is essential to ensure optimal power distribution to consumers. Otherwise, the frequency of the generating units will decline [1, 2]. When the amount of power generated falls below the needed level, the speed of the generator and frequency will begin to drop. As this happens over time, a mismatch between the output of energy and the load demand affects the voltage and frequency profiles [3, 4]. The electrical power system (PS) is a complex network composed of numerous electrical components. As the adoption of dynamic and intermittent nature, renewable energy sources (RES) has increased, designing a PS with sufficient frequency management has become a more significant challenge. Therefore, for the stable operation of power exchange in a complex power system with scores of utilities cross-connected through tie-lines and RES penetration, it is imperative to apply smart and intelligent approaches [5, 6]. Faced with these enormous challenges, the LFC system is considered the most notable alternative to delivering high-quality electricity to end users because of the complexities of the electrical network [7]. Hence, the principal objective of the LFC is to preserve an appropriate steadiness between production and power demand while keeping nonconformities in frequency and tie-line power changes within desired limits under various loads and disturbances. With the

LFC, the synchronous generators are driven to operate in response to load demand, thereby ensuring oscillations/errors in the tie-line and area frequencies/power are reduced to zero. A poorly designed LFC can result in undesirable huge fluctuations in the frequency and tie-line power tides, resulting in system instability and desynchronization [8]. Consequently, adopting a smart and intelligent-based control strategy for the LFC system becomes inexorable for engineers.

Researchers from around the globe are employing several schemes to manage the system's frequency and tie-line flow in both normal and disrupted scenarios [9]. Findings from the literature have shown that some control approaches such as classical control [10], adaptive control [11], optimal control [12], H-infinity control [13, 14], robust control [15], and internal model control [16] have been harnessed. However, in light of advances in nonlinearities and the integration of electronic components, IPSs require more advanced control techniques to supply adequate power output. Some other approaches have engaged the standard control methods, such as proportional-integral (PI) and proportional-integral derivate (PID) controllers for load frequency management [17, 18]. However, when considering the dynamic nature of the microgrid, these controllers are significantly sluggish, require longer computing time for suitable parameter estimation, and are inefficient in dynamic response [19]. In addition, the sole implementations of conventional PIDs and their variants cannot guarantee optimal LFC power management. As a result, a more sophisticated controller leveraging soft computing (SC) methods to optimize the PID gains and their variants are needed in attaining optimal performance. In comparison with conventional computing, soft computing approaches provide solutions for complex real-life problems and can handle approximate models. Consequently, previous works have considered harnessing SC with various types of PID variants.

Several works in the past have considered the use of classical controllers in addressing LFC problems. For instance, the proportional-integral (PI) controller [20] was harnessed to stabilize an IPS system with communication delay. The authors reported a better rejection response compared with other methods. Ali and Abd-Elazim [21] applied the bacterial foraging optimization algorithm (BFOA) for gain scheduling of a proportional-integral (PI) controller on a two-area non-reheat thermal system. Comparing the proposed method with other techniques, the output of the research indicated that the proposed system suppressed oscillations more effectively. A DE-based I/PI/PID control technique was introduced in [22]. The IPS was subjected to different test systems consisting of multisource units. The suggested DE-PID outshone its counterparts with the best dynamic response.

Shiva and Mukherjee [23] utilized a quasioppositional harmony search (QOHS)-based PID control scheme for a deregulated multiarea multisource IPS. With the extension of the areas of the IPS model and the integration of physical constraints such as time delay, generation rate constant (GRC), and governor dead band (GDB), the dynamics of the QOHS-based PID control framework gave superior performance compared to other methods. In a similar work, Guha et al. [24] optimally designed the PID controller using the quasioppositional grey wolf optimization algorithm (QOGWO). The integral time absolute error (ITAE) fitness function was adopted as the fitness function. According to the time domain analysis presented in the study, the proposed QOGWO-based PID controller outperformed fuzzy logic, artificial neural networks, and adaptive neuro-fuzzy interface system (ANFIS) controllers under diverse uncertainty conditions.

In a bid to design an effective LFC system, Shabani et al. [25] suggested a robust imperialist competitive algorithm (ICA)-based PID. The proposed ICA-based PID was implemented on three-area IPS while also being subjected to several load change conditions. The study showed that the ICA-based PID was more proficient than the genetic algorithm (GA)-based PI controller and neural network (NN) approaches. Also, authors in [26] have proposed the GA for selecting the gains of the conventional first-order PI controller. The PI controller which incorporates an inverse additive perturbation was formulated as an optimization problem to assure its robustness. The proposed robust PI controllable load and its robustness in the face of various disturbances and uncertainties have been verified through simulations on remote hybrid wind-diesel power systems.

In another work, Guha et al. [27] addressed the problem of the LFC system with two-area thermal PS by optimizing the parameters of the PI and PID with derivative filter a (PIDF) controller using the differential search algorithm (DSA). In [28], the GWO method was used to tackle the LFC problem in an IPS network using an existing PI/PID controller. The study is integrated with three other realistic IPS, involving a two-area nonreheat thermal-thermal power system with interconnections and a three-area interconnected thermal power system with interconnections. The proposed control strategy performed better than its competitors, according to the authors. Nevertheless, the last decade has seen modifiable versions of the PID controller widely used. For instance, Sahu et al. [29] explored the 2-degree freedom of a proportional-integral-derivative (2-DOF PID) controller on a two-area IPS. Considering the ITAE objective function, the suggested TLBO-based 2DOF PID outperformed the classical Ziegler-Nichols (ZN), GA, BFOA, DE, and hBFOA-PS-based PI controllers. A PID controller-based linear/nonlinear unified power system based on 2DOF PID was also investigated by Patel [30]. With the minimum value of the cost function, settling time, undershoot, and peak overshoot, the proposed cuckoo search algorithm (CSA)-based 2DOF PID exhibited a preferable dynamic response.

Daraz et al. [31] implemented an integral proportional derivative (I-PD) controller for a two-area multisource IPS. The recommended control strategy outperformed previous techniques with the shortest overshoot (O_{sh}), undershoot (U_{sh}), and settling time. A fractional-order fuzzy PID (FOFPID) controller was developed in [32] for the LFC of heterogeneous area IPS with dissimilar generating units. The outputs of the study indicated a better dynamic response than other methods. Several other variants have been reported in [33–36] to be effective in handling the LFC issues in an IPS.

1.2. Research Gap and Motivation. Findings have shown that the advent of modern PS networks has become significantly more complex, with many uncertainties present making the design of LFC a difficult task. The selection of secondary controller gains is another drawback of LFC designs. The system responses may be characterized by massive instantaneous oscillations, resulting in a wide area blackout, as a result of nonoptimal gain value selection [24, 37]. For remedying this problem, attempts have been made by combining different PID variants which is a form of cascade approach. The cascade control idea is well known for its capacity to quickly reject perturbations in the system before they impede the system [38]. They have proven to be more effective than conventional feedback controllers. Hence, a special cascade combination of 2DOF + FOPIDN and PD controllers, named (2DOF + FOPIDN)-PD controller, is considered and implemented for LFC in this study for the first time. Since the cascaded controller utilizes both 2DOF + FOPIDN and PD controllers, it harnesses the merits of the basic combined 2DOF – FOPID controller such as the ability to quickly reject disturbances while maintaining set-point tracking accuracy without considerably increasing overshoot. They can also be used to reduce the impact of changes with respect to the reference signal.

Another advantage of the projected controller is the degree of freedom. The primary functions of 2DOF controllers are to govern set-point tracking and disturbance rejection [39]. Furthermore, the proposed cascaded controller consists of the fractional-order integrodifferential operator. Therefore, given the aforementioned, this work proposes cascaded (2DOF – FOPIDN)-PD controllers for the LFC of IPS. The parameter settings for these new variants must be carefully optimized to get the best results on power system operations. Tuning a controller necessitates an in-depth understanding of the many parameters that determine the performance of the controlled system owing to the huge range of parameters that govern the controlled system. Achieving the most efficient gains for controllers requires a lot of effort and time [40].

Previous works indicate that a variety of nature-inspired optimization techniques were applied in LFC studies in order to gain maximum benefit from the controllers. For instance, works in references [6, 35] have recently applied nature-inspired algorithms for a multisource IPS using a set-point weighted fractional-order PID controller. However, one of the major distinctions between the reference [35] and the present work is that whereas the former work considered unequal areas with multisource power systems with the incorporation of GRC and GDB, this present work considered a more complex power system which incorporates both nonlinearities and the IPFC-RFBs coordination to enhance the system dynamic performance. In addition, whereas reference [6] applied a hybridized algorithm with a set-point weighted fractional-order PID controller, this study explored the use of a single and more recent algorithm that utilizes a coordinated Lévy flight and a modified inertia weight strategy.

Nevertheless, developing a successful algorithm requires striking a balance between diversity (search space exploration) and intensity (search space exploitation) [41]. An algorithm's exploration ensures that it utilizes the most viable portions of the search space, while its exploitation ensures that it finds the best solution within those regions. The fine-tuning of these components is necessary to find an optimal solution for a given problem. The honey badger algorithm (HBA) is a modern algorithm that has been shown to be effective. The HBA simulates the foraging behaviour of the honey badgers in digging and finding honey [42]. A metaheuristic approach cannot be ideally adapted to all problems, and there is always an opportunity for improvement, according to the "no-free lunch" theorem. Consequently, Lévy flight is therefore incorporated into the standard HBA to significantly increase its explorative capabilities so the improved algorithm can successfully traverse complex search spaces without becoming stuck at local optima (LO).

The application of Lévy flight (LF) has grown tremendously in different fields of life over the year. It has been utilized for optimization and optimal search of metaheuristic algorithms as evident in [43–46]. Supplementary alteration is carried out by incorporating an inertia weight into the components of the HBA. In all of these instances, the authors have reported an outstanding performance in the implementation of LF behaviour. The global search capability of the HBA increased with LF, which simulates a random walk with jump sizes determined by Lévy distribution.

1.3. Contribution and Paper Organization. The followings are the main contributions of this work:

(1) A newly structured (2DOF + FOPIDN)-PD cascade controller for the load frequency of an interconnected power supply system is proposed

(2) An improved honey badger algorithm by incorporating the concept of Lévy flight and inertia is designed to optimize the proposed controller

(3) The performance of the MHBA-tuned (2DOF + FOPIDN)-PD cascade controller in various load condition scenarios is investigated, and the simulation results demonstrate its superiority over other methods

(4) The robustness of the (2DOF + FOPIDN)-PD cascade controller for additional nonlinearities, electronics devices, system parameter variations, and random SLP is analysed

The following is the remainder of this paper: the materials and techniques, which include system modelling and controller structure, are presented in Section 2. Section 3 explains the HBA in general, whereas Section 4 presents the suggested method. Section 5 presents the findings and discussion. Finally, Section 6 presents the study's conclusion and future directions.

2. Materials and Methods

2.1. System Modelling. As shown in Figure 1, the power system under consideration consists of two areas with different energy sources: thermal (reheat), hydro and gas, and diesel plant units. Physical limitations, sometimes called nonlinear components, were taken into account in the suggested LFC. This is a key step in obtaining a valid result from a genuine power system. The multisource IPS then takes into account boiler dynamics as well as the GRC, which has a significant influence on the system's output. Figure 1 depicts the multisource IPS (MSIPS) transfer function model [35, 47–49]. The broiler dynamics is presented in Figure 2. In addition, tie-lines are used in conjunction with redox flow batteries (RFBs) and interline power flow controllers (IPFCs) in the proposed system.

Managing the IPFC and the RFB together, according to prior studies, increases dynamic system performance [50]. IPFCs are compensation converters from the FACTS series that regulate power flow across several lines on a single transmission line. The IPFC control units handle the regulating of multiple transmission line power flows. They are relatively new forms of flexible AC transmission systems (FACTS) control devices. The IPFC employed as a damping controller has a structure shown in Figure 3. On the other hand, redox flow batteries have received a lot of attention because of their exceptional qualities, which can be seen in their rapid reaction and flexibility, which are particularly evident during overloads. The redox flow batteries are controlled by the signal ACE. RFB, therefore, provides the regulating element to the load frequency regulation and greatly aids the linked power system's quality and flow. The block diagram of the redox flow battery is described in Figure 4.

At a nominal frequency of 60 Hz, each control area has a rating of 2000 MW and a nominal loading of 1000 MW. The tie-line connects the two MSIPS zones. As described in Figure 1, ΔACE_1 and ΔACE_2 denote the area control errors in both areas; the speed governor time constants are denoted as T_{G1} and T_{G2}, measured in seconds; the governor speed regulating parameters in p.u for region 1 are R_{H1} and R_{G1}; T_{T1} and T_{T2} are the turbine time constant for areas 1 and 2; B_1 and B_2 stand for frequency bias parameters; the changes in load are denoted by ΔPD_1 and ΔPD_2; K_{th1} and K_{th2} are the respective representation of the thermal constants; the IPS synchronization power coefficient is given as P_{12}; the speed governor constant of the diesel turbine is described as T_D; the marginal shift inline power (measured in p.u) is provided as ΔP_{Tie}, while the variations in frequency in area 1 and 2 are demonstrated as ΔF_1 and ΔF_2. The Appendix contains detailed parameters, and extensive equations may be found in [31, 35, 50, 51]. The error inputs to the controllers in areas 1 and 2 are denoted as follows:

$$\begin{aligned} ACE_1 &= B_1\Delta F_1 + \Delta P_{\text{tie1}-2,\text{error}},\\ ACE_2 &= B_2\Delta F_2 + \Delta P_{\text{tie2}-1,\text{error}},\\ \Delta P_{\text{tie2}-1,\text{error}} &= -\frac{P_{r1}}{P_{r2}}\Delta P_{\text{tie2}-1,\text{error}}. \end{aligned} \tag{1}$$

By seeing P_{r1} and P_{r2} as the rated power of the areas,

$$a_{12} = -\frac{P_{r1}}{P_{r2}}. \tag{2}$$

Then,

$$ACE_2 = B_2\Delta F_2 + a_{12}\Delta P_{\text{tie2}-1,\text{error}}, \tag{3}$$

where $\Delta\mathbf{F}_1$ and $\Delta\mathbf{F}_2$ symbolize the frequency variations in areas 1 and 2, respectively, $\Delta\mathbf{P}_{\mathbf{tie}}$ indicates the changes in tie-line power, and $\mathbf{B}_1$ and $\mathbf{B}_2$ represent the frequency bias parameters.

2.2. The Proposed Cascaded Controller Based on FOCs and 2DOF in the Power System

2.2.1. Overview of Fractional Order Calculus. Fractional order calculus (FOC) is as old as integer order calculus, but its application was limited to mathematics until recently [52]. Its applicability has piqued the curiosity of researchers in a variety of fields. In contrast to some conventional integer methods, FOC is better suited for modelling and analyzing real-time systems [53]. In recent years, fractional calculus has received a lot of attention in a variety of fields such as control systems, transmission line theory, heat-flux exchange, chemical analysis solutions.

One key benefit of fractional differintegrals is in their smart mechanism and their ability to take the memory and natural characteristics of copious things into account which is also a major advantage over traditional interorder calculus [54]. The fractional-order derivative is defined in three different ways: Riemann-Liouville (RL), Caputo, and Grunwald-Letnikov (GL). The RL definition is expressed in terms of the fractional integral as follows [55]:

$${}_{\alpha}D_t^{\alpha} f(t) = \frac{1}{\Gamma(n-\alpha)}\frac{d^n}{dt^n}\int_{\alpha}^{t}(t-\tau)^{n-\alpha+1} f(\tau)\mathrm{d}\tau, \tag{4}$$

where $(n-1) \le \alpha \le n$,n is an integer, α represents the real number, and $\Gamma(.)$ stands for Euler function. Also, the expression for RL for fractional integral is given as follows:

$$AD_t^{-\alpha} f(t) = \frac{1}{\Gamma(n)}\int_{\alpha}^{t}(t-\tau)^{\alpha-1} f(\tau)\mathrm{d}\tau, \tag{5}$$

where ${}_{\alpha}D_t^{\alpha}$ denotes the fractional operator. The Laplace domain R-L definition for the duo part can be expressed as follows [55]:

$$L\{{}_{\alpha}D_t^{-\alpha} f(t)\} = s^{\alpha}F(s) - \sum_{k=0}^{n-1} s^k\, {}_{\alpha}D_t^{\alpha-k-1} f(t)|_{t=0}, \tag{6}$$

where $(n-1) \le \alpha \le n$ and $L\{f(t)\}$ represent the Laplace transformation. The estimated s-transfer function of the fractional-order differentiator and integrator may be directly obtained using a variety of approximation methods. Using a recursive distribution of zeros and poles, Oustaloup et al. [56] offered a well-known estimate. Equation (7) illustrates a typical version of the Oustaloup approximation formulation within a frequency band for the fractional-order differentiator s^{α}.

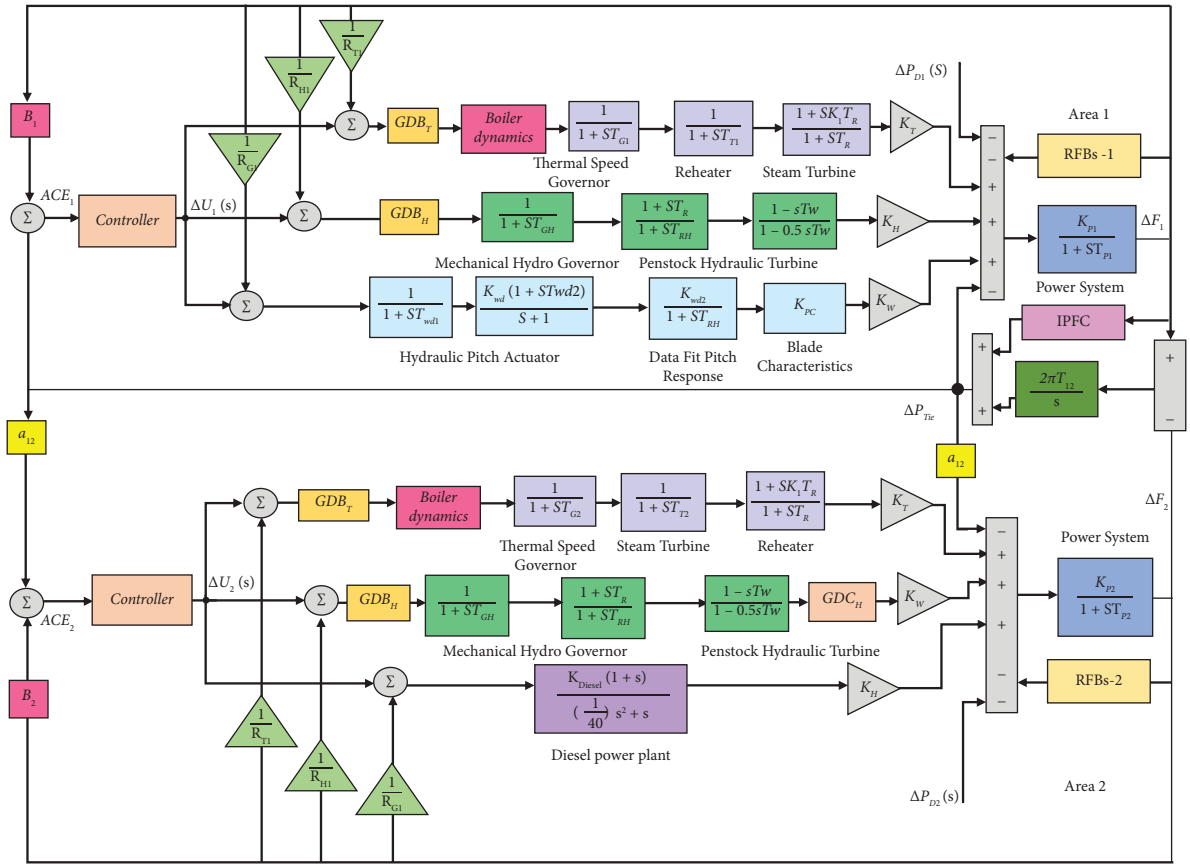

Figure 1: Transfer function model of the IPS under investigation.

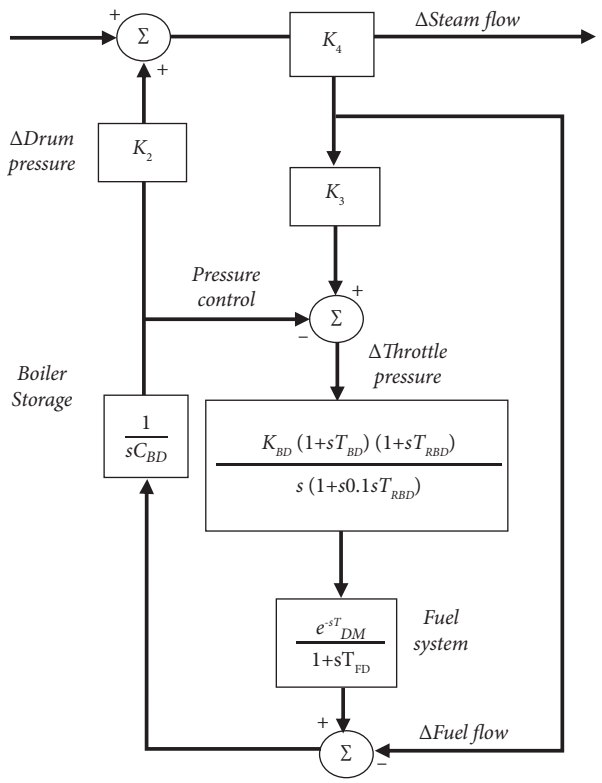

Figure 2: Boiler dynamics.

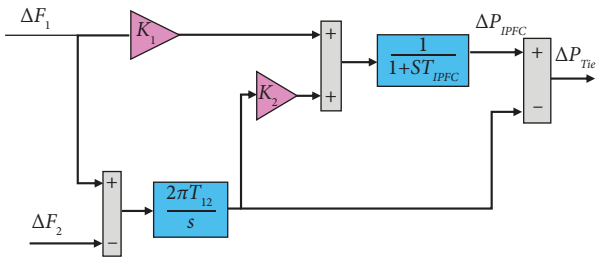

Figure 3: Structure of IPFC as damping controller.

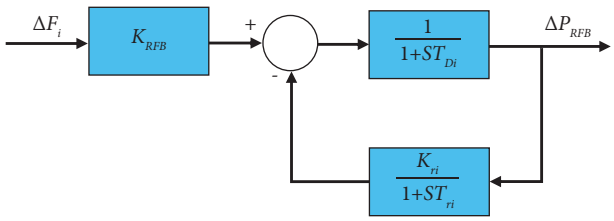

Figure 4: Block diagram of redox flow battery.

$$s^{\alpha} = K \prod_{k=-N}^{N} \frac{s + \omega_k'}{s + \omega_k}, \qquad \alpha > 0. \tag{7}$$

K is the feature gain that is kept to generate the unit gain at 1 rad/sec, as shown in equation (7). Poles and zeros have approximate frequencies of ω_k' and ω_k, respectively. ω_k' and ω_k denote the nominal pole and zero frequencies at the n^{th} instant having true values within the lower frequency (ω_b) and the high frequency (ω_h) of the system.

The filter's poles, zeros, and gain can be recursively calculated as follows:

$$\omega_k = \omega_b \left(\frac{\omega_h}{\omega_b}\right)^{(k+N+(1+\alpha)/2)/(2N+1)},$$
$$\omega_k' = \omega_b \left(\frac{\omega_h}{\omega_b}\right)^{(k+N+(1-\alpha)/2)/(2N+1)}, \tag{8}$$
$$K = \omega_h^{\alpha},$$

where α is the order of the differ-integration, and $(2N + 1)$ is the order of the filter. The frequency range used for this study is $\{10^{-3}, 10^{3}\}$ rad/sec with the order of the filter being the 5th order of Oustaloup's recursive approximation. Podlubny [57] devised a commonly used variant of the fractional-order PID controller that consists of an integrator order (λ) and a differentiator order (μ). Hence, the continuous transfer function of the fraction order (FO) controller is defined as follows:

$$G(s) = K_p + \frac{K_i}{s^{\lambda}} + K_d s^{\mu}. \tag{9}$$

The FOPID controller features two extra parameters (integral-order and derivative-order) in addition to the fundamental three (K_P, K_I, and K_D) of the normal PID controller, which are responsible for its versatility and durability. The FOMCON toolbox in MATLAB is utilized in this work to implement the proposed controller.

2.2.2. Cascade (2DOF + FOPIDN)-PD Controller Structure. Control systems with cascade controllers offer better set-point tracking and disturbance removal. They can be used to mitigate the effects of changes in the reference signal on the control signal. A cascade controller differs from conventional controllers in that it has two loops, the primary (inner/slave) loop and the outer (secondary/master) loop. It is much faster for the inner loop to respond than the outer loop, so disturbances within the loop can be reduced before they spread elsewhere in the system. This study presents a single-loop control system with a 2DOF + FOPIDN-PD controller and a cascade control system with a PD controller. The outer and inner controllers are here designated as $C_1(s)$ and $C_2(s)$. As expressed in (10) and (11), whereas the 2DOF + FOPIDN is selected as the outer controller, the PD controller is classified as the inner controller.

$$C_1(s) = K_P + \frac{K_I}{s^{\lambda}} + K_d s^{\mu}\left(\frac{N}{N + s^{\mu}}\right), \tag{10}$$

$$C_2(s) = K_P + K_d(s). \tag{11}$$

The description of the block diagram of the control system with the cascade controller is shown in Figure 5, while the overall closed-loop transfer function is presented in the following equation [58]:

$$Y(s) = \left[\frac{G_1(s)G_2(s)C_1(s)C_2(s)}{1 + G_2(s)C_2(s) + G_1(s)G_2(s)C_1(s)C_2(s)}\right]R(s) + \left[\frac{G_1(s)}{1 + G_2(s)C_2(s) + G_1(s)G_2(s)C_1(s)C_2(s)}\right]d_1(s), \tag{12}$$

where $G_1(s)$ is the primary control loop; $G_2(s)$ is the secondary control loop; $d_1(s)$ is the load disturbance.

2.3. Objective Function. Performance criteria are quantitative measures of a control system's effectiveness [59]. The device's ability to accomplish the prerequisites of the controller's design is demonstrated by an objective function that details its proficiency. Numerous performance metrics, including integral squared error (ISE), integral time-weighted absolute error (ITAE), integral time multiply squared error (ITSE), and integral absolute error (IAE), have been effectively used to evaluate the performance of a conventional PID controller [60]. A significant part of achieving optimized parameters entails

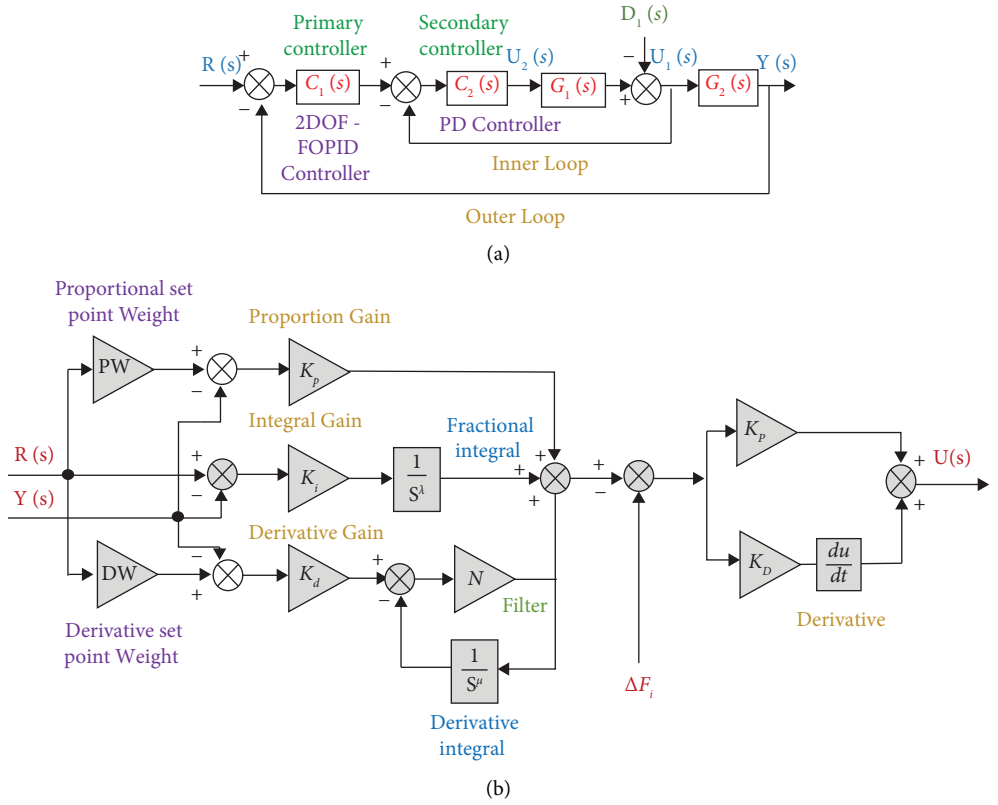

Figure 5: Different components of the system. (a) Block diagram of cascade controller. (b) 2DOF + FOPIDN-PD controller structure.

minimizing the fitness function. To guarantee optimal dynamic performance, the controller settings should be configured with a minimal overshoot, undershoot, and settling time. Because of the ITSE's squared error, big oscillations are penalized more severely, making it feasible to reduce significant oscillations in frequency and tie-line fluctuations. In order to display the performance of controllers, the proposed algorithm uses the ITSE. Equation (13) describes the ITSE mathematically.

$$\mathbf{J = ITSE} = \int_0^{\mathbf{T}} \left((\Delta \mathbf{F_i})^2 + (\Delta \mathbf{P_{Tie-i-k}})^2 \right) \mathbf{tdt}, \tag{13}$$

where ΔF_i and t are the respective frequency deviation in area i and the simulation time; the shift in tie-line power linked between area i and k is denoted as $\Delta P_{\text{Tie}-i-k}$. By minimizing J giving to the following constraints, the proposed cascaded (2DOF + FOPIDN)-PD controller parameters are optimized by the MHBA algorithm.

Minimize the objective function = J (14), subject to

$$\begin{aligned}
&K_{Pi}^{\min} \le K_{Pi} \le K_{Pi}^{\max}; K_{Ii}^{\min} \le K_{Ii} \le K_{Ii}^{\max}; K_{Di}^{\min} \\
&\quad \le K_{Di} \le K_{Di}^{\max}; \\
&K_{P2i}^{\min} \le K_{P2} \le K_{P2i}^{\max}; K_{D2i}^{\min} \le K_{D2} \le K_{D2i}^{\max}; N_{I\min} \\
&\quad \le N_I \le N_{I\max}; \\
&\mu_i^{\min} \le \mu_i \le \mu_i^{\max}; \lambda^{\min} \le \lambda \le \lambda^{\max}; PW_{I\min} \\
&\quad \le PW_I \le PW_{I\max}; \\
&DW_{I\min} \le DW_I \le PW_{I\max},
\end{aligned} \tag{14}$$

where the superscripts min and max represent the minimum and maximum values of the controller parameters, respectively.

3. Background

3.1. Honey Badger Algorithm (HBA). The honey badger algorithm (HBA) is a recent and innovative algorithm proposed by Hahim et al. [42] in 2021. The HBA model is based on honey badger foraging behaviour, with exploration and exploitation stages modelled after digging and hunting for honey. The operation of the HBA is classified into two different phases. Phase one is known as "digging" and is characterized by the use of a honey badger's smelling ability to determine the location of prey. Once the honey badger reaches its prey, it begins the second stage, which is called the "honey phase." By moving around its prey, the honey badger picks just the right spot for digging and catching it. In the latter mode, the honey badger uses a honeyguide bird as a guide in order to find a beehive. The HBA involves several steps, which are summarized as follows [42]:

Step 1: Initialization Phase. The number (population size N) and the positions of the honey badgers are initialized as shown in equation (19)

$$x_i = lb_i + r_1 \times (ub_i - lb_i), \tag{15}$$

where the random number r_1 varies between 0 and 1; x_i implies the i th honey badger position referring to a

candidate solution in a population of N; lb_i and ub_i are lower and upper bounds of the search area, respectively.

Step 2: Defining Intensity (I). The intensity of a hunt is determined by the concentration strength of the prey and the distance between it and i^{th} honey badger. The smell intensity of the prey is denoted as I_i; during an increased smell, the motion becomes fast, and vice versa, which is in a similitude of the inverse square law [61] which can be expressed by equation (16).

$$\begin{aligned} I_i &= \left(r_2 \times \frac{S}{4\pi d_i^2}\right), \\ S &= \left(x_i - x_{i+1}\right)^2, \\ d_i &= \left(x_{\text{prey}} - x_i\right), \end{aligned} \tag{16}$$

where the random number r_2 varies between 0 and 1; S represents the strength or concentration strength; d_i signifies the distance between the prey and the i th badger.

Step 3: Update Density Factor. The density factor (α) is responsible for controlling the time-varying randomness of exploration and ensuring smooth transitions between the exploratory and exploitation phases. Equation (21) is utilized to update the decreasing factor α which declines with iterations and consequently decreases randomization over time.

$$\alpha = C \times \exp\left(\frac{-t}{t_{\max}}\right), \tag{17}$$

where C is a constant ≥1, and $t_{\max}$ is the maximum number of iterations.

Step 4: Escaping from LO. The current step, as well as the two stages after it, is utilized to escape the LO zone. The proposed algorithm utilizes an F flag that alters the search direction for agents to be able to thoroughly peruse the search space.

Step 5: Updating the Agents' Positions. According to the former explanation, HBA position updates (x_{new}) are separated into two stages–the "digging phase" and the "honey phase." These essential stages are discussed as follows.

Step 5(a): Digging Phase. A honey badger digs in a manner that is comparable to the cardioid shape represented in equation (18) [42]:

$$\begin{aligned} x_{\text{new}} = {} & x_{\text{prey}} + F \times \beta \times I \times x_{\text{prey}} \\ & + F \times r_3 \times \alpha \times d_i \times \left|\cos\left(2\pi r_4\right)\right. \\ & \left. \times \left[1 - \cos\left(2\pi r_5\right)\right]\right|, \end{aligned} \tag{18}$$

where x_{new} is the global best; β is the honey badger's capacity to obtain food ($\beta \geq 1$); the distance between the prey and the i^{th} honey badger is depicted as d_i; r_3, r_4, and r_5 represent a range of random values between 0 and 1. The flag F is used to change the search direction and is calculated by

$$F = \begin{cases} 1 & \text{if } r_6 \leq 0.5 \\ -1 & \text{else.} \end{cases} \tag{19}$$

The honey badger is profoundly impacted by three key parts in the digging stage: smell intensity I of prey x_{prey}, the distance between the badger and its prey d_i, and time-varying search influence factors. It is worth noting that badgers may experience a disturbance F during digging operations, allowing them to pursue prey in even better positions [42].

Step 5(b): Honey Phase. Equation (24) represents the circumstance in which a honey badger follows the honeyguide bird to a beehive.

$$x_{\text{new}} = x_{\text{prey}} + F \times r_7 \times \alpha \times d_i, \tag{20}$$

where r_7 is an arbitrary number somewhere in the range of 0 and 1; x_{new} is the prey location; F and α are obtained from equations (17) and (19). From equation (24), a honey badger searches close to the prey location x_{prey} where it has already found prey by using distance information d_i; search behaviour at this point varies with time (α). The pseudocode of the standard HBA is presented in Figure 6.

3.2. Lévy Flight. Lévy flight (LF) was initiated in 1937 by Paul Lévy, a French mathematician at the time. Detailed explanations of the concept were later provided by Benoit Mandelbrot. The LF describes motion in a more comprehensive way than the much earlier Brownian motion [43]. LFs are non-Gaussian random walks featuring steps generated from a Lévy distribution. The distribution referred to is a basic power-law formula $L(s) \sim |s|^{-1-\beta}$ where $0 < \beta < 2$ is an index formula [62]. Numerous studies have demonstrated that many animals and insects exhibit LF-like characteristics during flight [44]. With reference to [63], fruit flies or *Drosophila melanogaster* explore their landscape by means of a series of direct routes marked by a sudden turn of 90°C which triggers an irregular scale-free Lévy-style search pattern (see Figure 7).

This is evident in the way they seek food by randomly moving from place to place [65]. A simplified version of the Lévy distribution can be described mathematically as follows [66]:

$$L(s, \lambda, \mu) = \begin{cases} \sqrt{\dfrac{\gamma}{2\pi}} \exp\left[-\dfrac{\gamma}{2(s-\mu)}\right] \dfrac{1}{(s-\mu)^{3/2}} & \text{if } 0 < \mu < s < \infty \\ 1 & \\ 0, & \text{if } s \leq 0, \end{cases} \tag{21}$$

where the location or shift parameter is denoted as μ; the control of the scale distribution is enabled by the parameter. $\gamma > 0$.

Set parameters t_{max}, N, β, C
Initialize population with random positions
Evaluate the fitness of each honey badger position x_i *using objective function and assign to* f_i, $i \in [1,2,\ldots,N]$.
Save the best position x_{prey} *and assign fitness to* f_{prey}.
while $t \leq t_{max}$ ***do***
  Update the decreasing factor α *using Eq. (17)*
  for $i = 1$ *to* N ***do***
    Calculate the intensity I_i *using Eq. (16)*
    if $r < 0.5$ ***then***
      Update the position x_{new} *using Eq. (18)*
    else
      Update the position x_{new} *using Eq. (20)*
    end if
    Evaluate new position and assign to f_{new}
    if $f_{new} \leq f_i$ ***then***
      Set $x_i = x_{new}$ *and* $f_i = f_{new}$
    end if
  end for
end while *Stop criteria satisfied*
Return x_{prey}

Figure 6: Pseudocode of HBA [42].

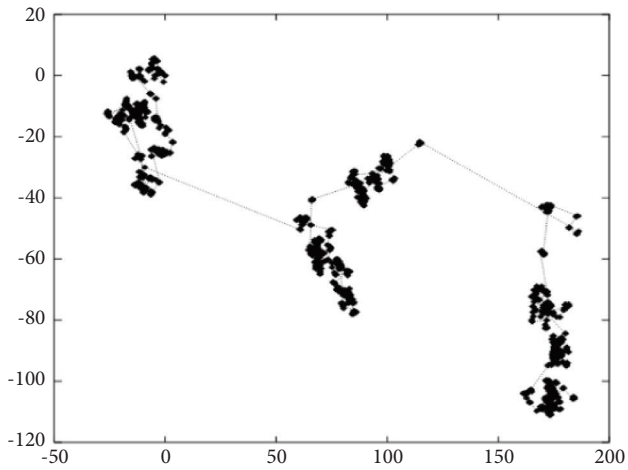

Figure 7: Simulations tracks of Lévy flight [64].

A Lévy distribution can be represented using the Fourier transform [62]:

$$L(k) = \exp\left[-\propto |k|^{\beta}\right], 0 < \beta \leq 2, \tag{22}$$

where $\propto$ is the skewness or scale factor and has a number in the interval of $[-1, 1]$; β is the Lévy index also known as the index of stability and is given as $\beta \in [0, 2]$. According to [62], except perhaps for a few rare circumstances, the analytic form of the integral is unknown in general. The integral may be determined analytically in the case of $\beta = 1$ and is known as the Cauchy probability distribution [62].

$$F(k) - \exp[-\propto |k|]. \tag{23}$$

In another scenario, when $\beta = 2$, the distribution corresponds to a Gaussian distribution and can be expressed as follows:

$$L(k) = \exp\left[-\propto |k|^2\right]. \tag{24}$$

It is worth noting that the parameters β and $\propto$ are paramount in determining the distribution. It is possible to obtain different shapes of the probability distribution by varying parameter β in a manner that makes it possible to control the tail region of the probability distribution.

4. The Proposed Approach (MHBA)

The honey badger algorithm (HBA) replicates the honey badger's ability to detect prey by strolling slowly and persistently while employing sniffing mouse abilities. The process of digging for prey eventually leads to finding out its approximate location prior to catching it. As part of its foraging efforts, it can dig up to fifty holes within a radius of forty kilometers in a single day [42]. Although the honey badger enjoys honey, it does not possess the adequate capability to locate beehives. Consequently, honey badgers are dependent on the honeyguide (a bird) which can find hives. This made the HBA population remains susceptible to local optima (LO) stagnation in some circumstances, resulting in unsatisfactory results because of immature convergence. A seamless transition from the exploration to exploitation phases cannot always be achieved with the standard HBA algorithm. The concept of Lévy flight (LF) can be utilized to alleviate the aforementioned problems. The LF mechanism is then integrated to increase and balance the algorithm's search capabilities via a deeper searching pattern. Through this method, global searching can be handled more efficiently and avoids LOs altogether. Moreover, an inertia

Set parameters t_{max}, N, β, C, ω
Initialize population with random positions
Evaluate the fitness of each honey badger position x_i *using objective function and assign to* f_i, $i \in [1,2,\ldots,N]$.
Save the best position x_{prey} *and assign fitness to* f_{prey}.
while $t \leq t_{max}$ ***do***
  Update the decreasing factor α *using Eq. (17)*
  for $i = 1$ *to* N ***do***
    Calculate the intensity I_i *using Eq. (16)*
    if $r < 0.5$ ***then***
      Update the position x_{new} *using Eq. (18)*
    else
      for each search agent
      Update the position x_{new} *using Eq. (25)*
    end if
    Evaluate new position and assign to f_{new}
    if $f_{new} \leq f_i$ ***then***
      Set $x_i = x_{new}$ *and* $f_i = f_{new}$
    end if
  end for
end while *Stop criteria satisfied*
Return x_{prey}

Figure 8: Pseudocode of the proposed MHBA.

weight is incorporated as a way to enhance time-varying randomization and prevent jarring transitions between exploration and exploitation. Therefore, the LF is used to update the honey badger position as follows:

$$x_{\text{new}} = x_{\text{prey}} + \omega \times F \times r_7 \times \alpha \times d_i \otimes \text{Lévy}, \quad (25)$$

where x_{new} is the prey location; r_7 is an arbitrary number somewhere in the range of 0 and 1, flag F is represented as F, ω is the inertia weight as shown in equation (26); α is the density factor (α); the product $\otimes$ is the entry wise multiplication.

By introducing initial weight (ω), given in equation (26), more improvement is incorporated at the honey phase to reinforce the scope of search during the exploration phase of the algorithm. As a result, a suitable adjustment would aid in ensuring the diversity of honey badges, preventing inadequate convergence, and increasing the algorithm's effectiveness [67]. The inertia weight is a modified linear decreasing inertia weight as presented in [68], which can be expressed as follows:

$$\omega = \left(\omega_{\text{start}} - \omega_{\text{end}}\right)\left(\frac{T_{\max} - t}{T_{\max}}\right) + \omega_{\text{end}} \times e^{-\left(t/T_{\max}/4\right)^2}, \quad (26)$$

where t is the present iteration, $T_{\max}$ is the maximum iteration, and w_{start} and w_{end} are given as 0.9 and 0.4, respectively.

The stochastic (27) determines the probability of a random walk, which enables the proposed MHBA to escape LO and ensures that the search agent (honey badger) can sufficiently traverse the search space. According to the Lévy flight, a random walk has the following distribution [69]:

Table 1: Algorithm parameters.

Algorithm	Parameter	Value
PSO [6]	C_1	2.0
	C_2	2.0
	$w_{\min}$	0.9
	$w_{\max}$	0.2
HBA	Beta	6
	C	2
GA	Crossover rate	0.8
	Selection mechanism	Roulette wheel
MFO	a	−1
	b	1
	C	2
MHBA	$w_{\min}$	0.9
	$w_{\max}$	0.4
TLBO [6]	N/A	NA

NA-not applicable

$$\text{Levy} \sim t^{-\delta}, 1 < \delta \leq 3. \quad (27)$$

The Lévy flight was developed by Paul Levy in 1937 by extending Brownian motion to include non-Gaussian randomly distributed step sizes [70]. As shown in Figure 6, it is a graphic depiction of Lévy flights' simulation tracks, which are characterized by small steps most of the time but with occasional larger ones. Using Menegna's [71] algorithm, random step lengths s are generated that behave like Lévy flights in order to mimic a λ-stable distribution. This can be represented as follows:

$$s = \frac{\mu}{|\nu|^{1/\beta}}, \quad (28)$$

Table 2: Controllers' optimal parameters.

		GA	TLBO [6]	MFO	PSO [6]	HBA	MHBA
Area 1	K_{p1}	1.9038	1.7465	2.9032	1.7471	2.7106	1.8134
	K_{i1}	2.4658	2.0000	2.1214	1.7093	3.0000	1.6521
	K_{d1}	2.7111	2.0000	2.4376	1.9857	1.5000	2.3707
	PW_1	—					1.9879
	DW_1	—					1.9785
	K_{P1}	—					5.0031
	K_{D1}	—					5.4745
	λ_1	—					0.9870
	μ_1	—					0.9790
	N_1	—					229.2756
Area 2	K_{p2}	2.3970	1.7627	1.9550	1.7471	1.5000	1.8850
	K_{i2}	2.6355	1.7736	2.2252	1.7093	3.0000	2.0635
	K_{d2}	1.8209	1.8842	1.7497	1.9857	1.8491	2.4718
	PW_2	—					1.9796
	DW_2	—					1.9685
	K_{P2}	—					4.3495
	K_{D2}	—					4.2896
	λ_2	—					0.9910
	μ_2	—					0.8798
	N_2	—					153.2224

where s is the step length, and μ and v are fashioned with respect to normal distributions:

$$\mu \sim N\left(0, \sigma_\mu^2\right), \quad v \sim N\left(0, \sigma_V^2\right), \tag{29}$$

with

$$\sigma_\mu = \left[\frac{\Gamma(1+\beta) \times \sin(\pi \times \beta/2)}{\Gamma(((1+\beta/2) \times \beta \times 2^{(\beta-1)/2}}\right]^{1/\beta}, \quad \sigma_v = 1. \tag{30}$$

The random walk of Lévy provides an improved global search competence of the HBA. This will enable the proposed algorithm to achieve a good balance between exploration and exploitation. The algorithm accesses the beneficial areas within the search space by exploring (diversifying), and the search for optimum solutions inside the region is assured by exploitation (intensifying). To develop an ideal solution for a specific situation, these components must be fine-tuned. Thus, the modified Lévy-based HBA is suggested to have more advantages than the conventional HBA for avoiding being trapped in the LO and for achieving excellent results. The pseudocode for the proposed HBA is shown in Figure 8.

5. Results and Discussion

The modelling and simulation of the LFC of the IPS under consideration were performed in MATLAB version 9.6 (R2019a). Figure 1 shows a typical load demand situation for a power plant in each area for thermal, hydro, wind, and diesel power sources. The numerical data used for the system may be found in the Appendix. As shown in Table 1, the parameter settings for the proposed algorithm and the other algorithms compared in this study are listed, while Table 2 describes the suggested controller's optimal settings compared and also for others. In order to identify and design fractional-order (FO) controllers, we used the FOMCON toolbox of MATLAB [72]. The total number of runs, population size (*NP*), and the total number of iterations are 10, 30, and 50, respectively. The performance of the proposed control scheme is compared with other methods such as PSO : PID [6], GA : PID, HBA : PID, TLBO : PID [6], and MFO : PID. Dynamic response performance is analysed using the ITSE index, settling time, and undershoot.

5.1. Load Changes. In this session, the response of the IPS which includes physical constraints and IPFC-RFBs coordination under different load conditions is described.

(a) Scenario 1: The initial stage of the test involves increasing the load in Area 1 by 0.1 p.u with no load change in area 2. Figures 9(a)–9(c) detail the dynamic response of the system with diverse controllers under this scenario. Table 3 describes the transient response outputs of the frequency deviations in areas 1 and 2 (ΔF_1 and ΔF_2), as well as the tie-line deviation (ΔP_{Tie}). Table 3 reveals the minimal value of the cost function, and J is exhibited by the proposed MHBA-tuned (2DOF + FOPIDN)-PD (ITSE = $9.2560e-04$) in comparison with GA-optimized PID (ITSE = 0.0686), TLBO-optimized PID (ITSE = 0.0776) [6], MFO-optimized PID (ITSE = 0.0526), HBA-optimized PID (ITSE = 0.2087), and PSO optimized PID (ITSE = 0.0851) [6]. Similarly, Figures 9(a)–9(c) illustrate the performance comparison between the proposed method and other methods, indicating that the performance of the MHBA-tuned (2DOF + FOPIDN)-PD reached the steady state

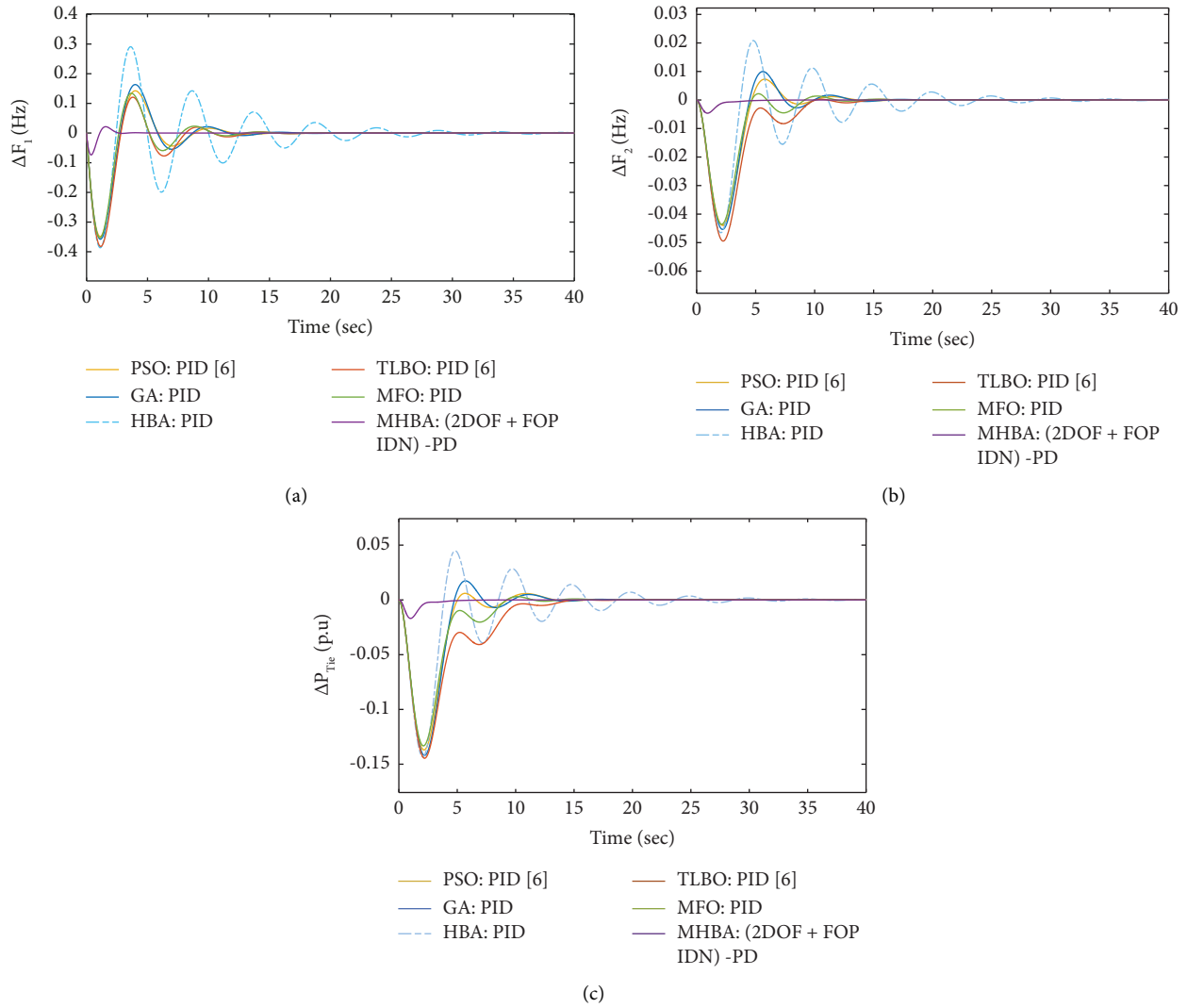

Figure 9: Dynamic performance of the IPS model for scenario 1 (a) ΔF_1, (b) ΔF_2, and (c) ΔP_{Tie}.

Table 3: Performance index of various techniques for scenario 1.

Controllers	ITSE	Settling time (s) (T_s)			Undershoot (U_{sh})		
		ΔF_1	ΔF_2	ΔP_{tie}	ΔF_1	ΔF_2	ΔP_{tie}
GA:PID	0.0686	13.3307	12.3271	12.1947	0.2012	0.1624	0.1433
TLBO:PID [6]	0.0776	13.0450	14.1876	14.1876	0.2325	0.1412	0.1660
MFO:PID	0.0526	11.9993	10.9559	10.422	0.8547	0.1346	0.1161
HBA:PID	0.2087	29.2135	27.8100	25.2838	0.7457	0.4058	0.1063
PSO:PID [6]	0.0851	13.3972	12.1960	12.1960	0.1287	0.1099	0.1387
MHBA(2DOF + FOPIDN)-PD	9.2560e-04	2.5047	6.4311	6.3718	0.1592	0.0291	0.0307

more rapidly with the shortest settling time, $T_s(\Delta F_1 = 2.5047$; $\Delta F_2 = 6.4311$; $\Delta P_{\text{tie}} = 6.3718)$, and undershoots, U_{sh} ($\Delta F_1 = 0.1592$; $\Delta F_2 = 0.0291$; $\Delta P_{\text{tie}} = 0.0307$), without oscillations than other methods in contrast with other methods. From this perspective, the proposed control method provides a more proficient control scheme.

(b) Scenario 2: a step load increases in Area 1 with a step load decreases in area 2. In this scenario, the step load in area 1 is increased by 0.1 p.u, while the load in area 2 is decreased by 0.05 p.u. The performance of the various controllers is compared to the suggested technique in Figures 10(a)–10(c). It is obvious from Table 4 that the minimum ITSE error is obtained with the MHBA-tuned (2DOF + FOPIDN)-PD controller (ITSE = 0.0668) in contrast with other methods used in the comparison. In the same vein, Table 4 shows that the minimum settling time, T_s,

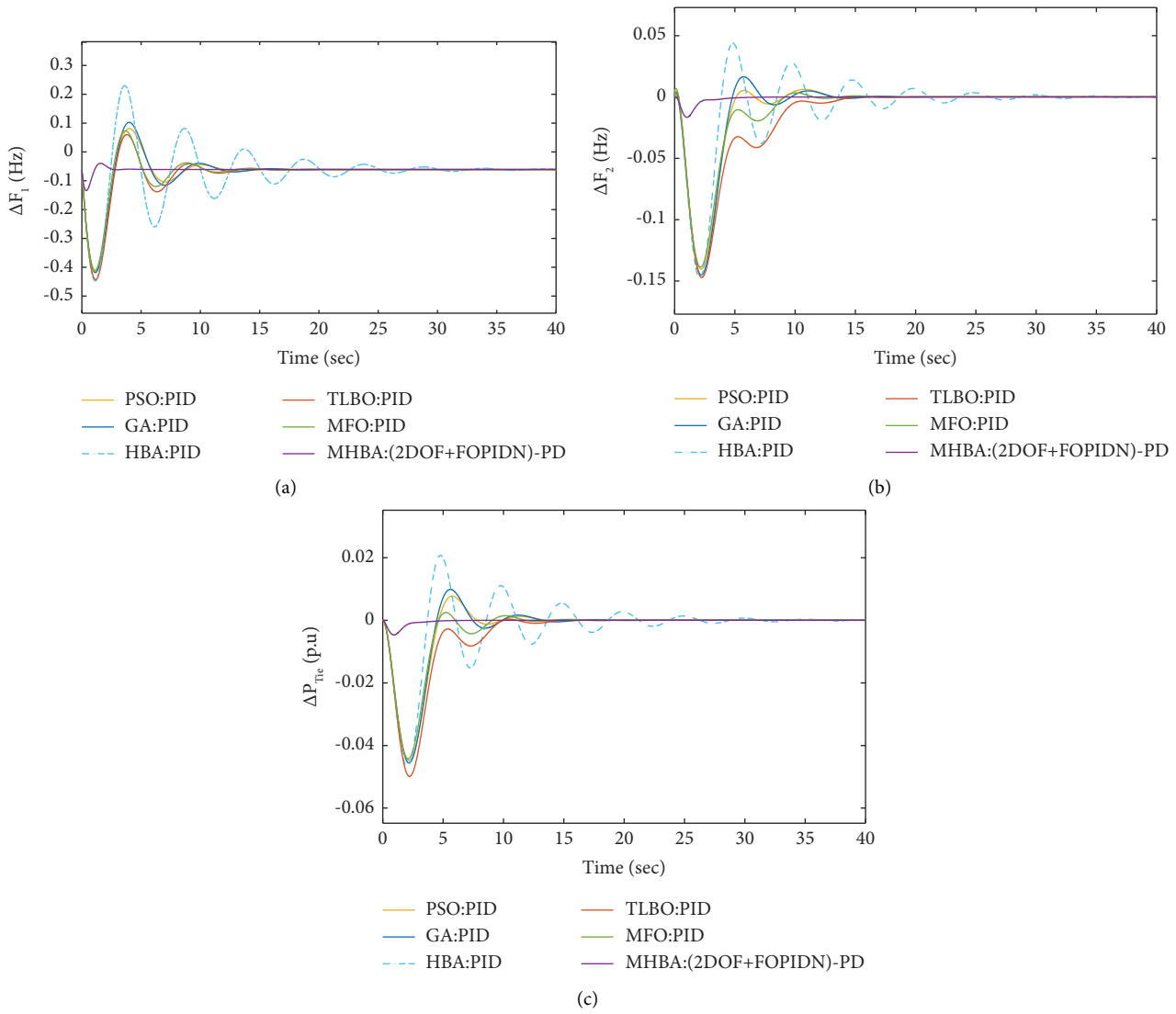

Figure 10: Dynamic performance of the IPS model for scenario 2 (a) ΔF_1, (b) ΔF_2, and (c) ΔP_{Tie}.

Table 4: Performance index of various techniques for scenario 2.

Controllers	ITSE	Settling time (s) (T_s)			Undershoot (U_{sh})		
		ΔF_1	ΔF_2	ΔP_{tie}	ΔF_1	ΔF_2	ΔP_{tie}
GA : PID	0.06680	13.2782	12.1506	12.2873	0.1959	0.1465	0.1630
TLBO : PID	0.07091	12.4105	13.5080	12.8764	0.8080	0.0911	0.1093
MFO : PID	0.05262	11.9856	10.5166	10.9705	0.1404	0.1208	0.1367
PSO : PID	0.05962	11.2687	12.2544	12.1972	0.1697	0.1375	0.1558
HBA : PID	0.20190	29.1812	25.1967	27.7462	0.3113	0.9419	0.0701
MHBA(2DOF + FOPIDN)-PD	$9.2590e-04$	2.5055	6.4416	6.1535	0.1593	0.0300	0.0294

belongs to the MHBA-tuned (2DOF + FOPIDN)-PD ($\Delta F_1 = 2.5055$; $\Delta F_2 = 6.4416$; $\Delta P_{\text{tie}} = 6.1535$). A better response is also reiterated in the magnitude of the undershoots, U_{sh} ($\Delta F_1 = 0.1593$; $\Delta F_2 = 0.0300$; $\Delta P_{\text{tie}} = 0.0294$).

5.2. Dynamic Response of the IPS with Physical Constraints and IPFC Only. In this subsection, the proposed IPS is examined without the inclusion of the RFBs to further explore its efficacy. As shown in Figures 11(a)–11(c), the suggested solution had lesser damping and an evener curve,

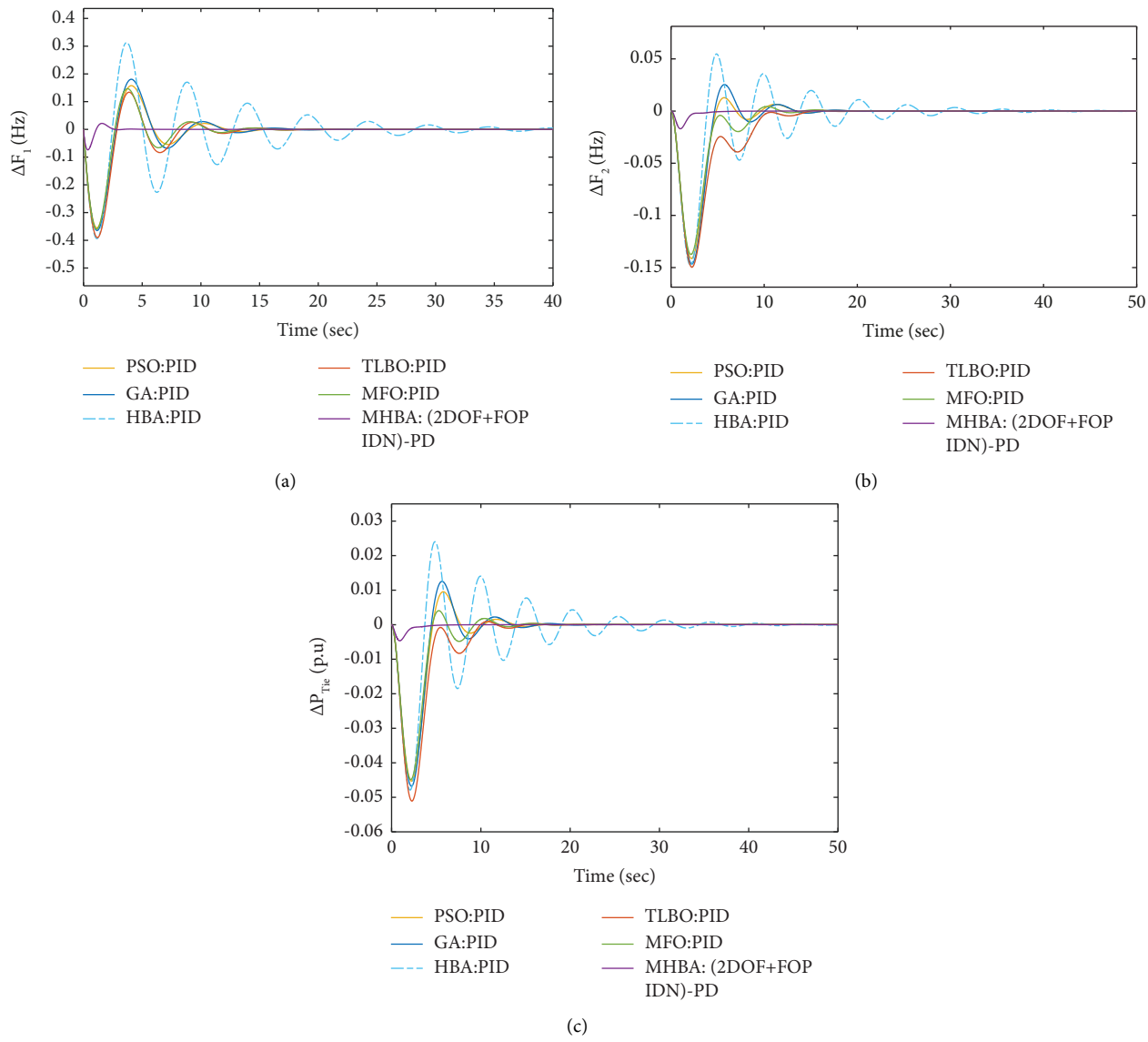

Figure 11: Dynamic performance of the IPS model with IPFC only (a) ΔF_1, (b) ΔF_2, and (c) ΔP_{Tie}.

Table 5: Performance index of various techniques with IPFC only.

Controllers	ITSE	Settling time (s) (T_s)			Undershoot (U_{sh})		
		ΔF_1	ΔF_2	ΔP_{tie}	ΔF_1	ΔF_2	ΔP_{tie}
GA : PID	0.08201	14.0647	12.6466	12.7716	0.2216	0.1480	0.1674
TLBO : PID	0.08015	12.8564	13.7882	13.3686	0.1007	0.0926	0.1119
MFO : PID	0.05965	12.5009	11.0403	11.3726	0.1556	0.1197	0.1385
PSO : PID	0.06927	13.939	12.5979	12.7963	0.1884	0.1385	0.1574
HBA : PID	0.30010	37.3795	30.8181	33.3722	0.6440	1.1272	0.1052
MHBA (2DOF + FOPIDN)-PD	0.00090	2.5138	6.3595	6.4189	0.0075	0.0308	0.0292

as well as being immediately driven down to zero when compared to other approaches. Also, as reported in Table 5, the minimal values of the ITSE (0.0009) belong to MHBA-tuned (2DOF + FOPIDN)-PD and the best values of the settling time, t_s (ΔF_1 = 2.5138; ΔF_2 = 6.3595; ΔP_{tie} = 6.4189), and undershoot, U_{sh}(ΔF_1 = 0.0075; ΔF_2 = 0.0308; ΔP_{tie} = 0.0292). In consequence, this technique is able to reduce the frequency and tie-line fluctuations with greater rapidity as evidenced by the smaller values of its cost function (*ITSE*), settling time (t_s), and undershoot (U_{sh}).

The ITSE values for all of the situations studied are compared in Figure 12. Compared to other techniques, the suggested control scheme kept the cost functions' minimum values. So far, the combined responses have demonstrated

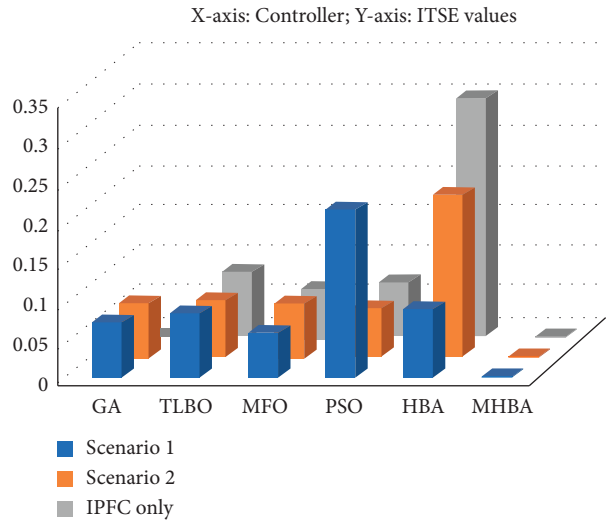

Figure 12: Performance index J (ITSE) comparison for all the cases.

Table 6: The IPS sensitivity analysis.

Parameter variation	% Change	Settling time $T_s(s)$			Undershoot U_{sh}		
		ΔF_1	ΔF_2	ΔP_{tie}	ΔF_1	ΔF_2	ΔP_{tie}
Nominal	0	2.7035	6.8208	6.8752	0.0213	0.0428	0.0418
T_G	−25	2.7036	6.8210	6.8754	0.0213	0.0428	0.0418
	+25	2.7034	6.8205	6.8750	0.0213	0.0428	0.0418
T_R	−25	2.4453	9.4298	9.5691	0.0179	0.0281	0.0287
	+25	2.4464	9.4311	9.5710	0.0180	0.0282	0.0287
R	−25	1.5949	10.0042	10.0851	0.0212	0.0053	0.0051
	+25	1.5925	10.0763	10.0715	0.0212	0.0052	0.0050

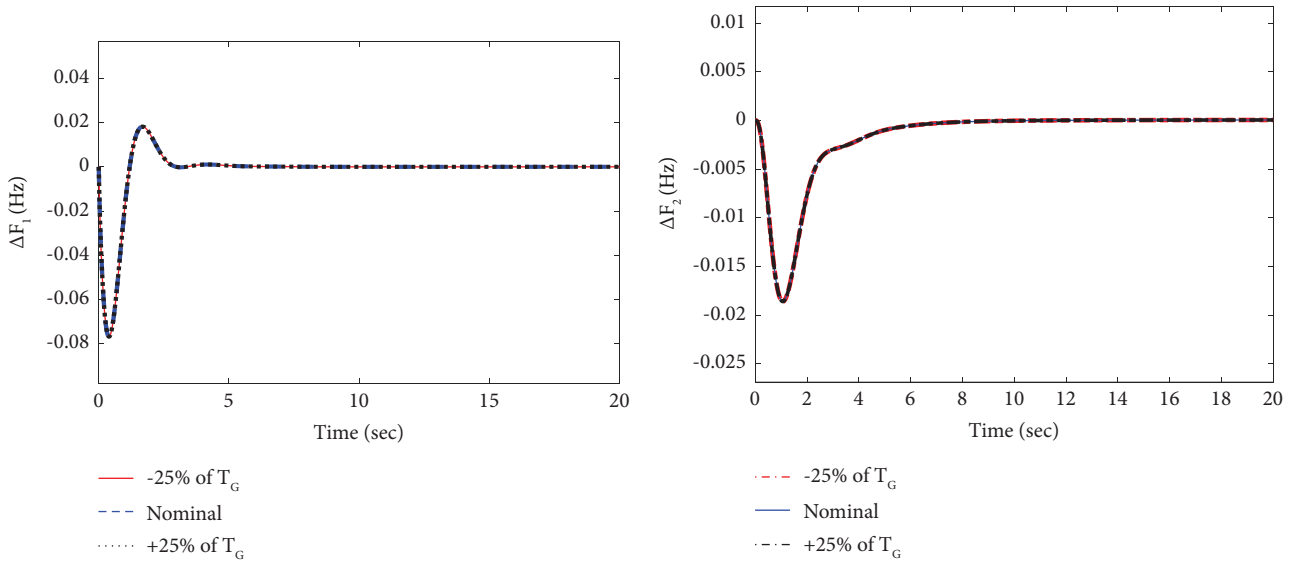

Figure 13: Continued.

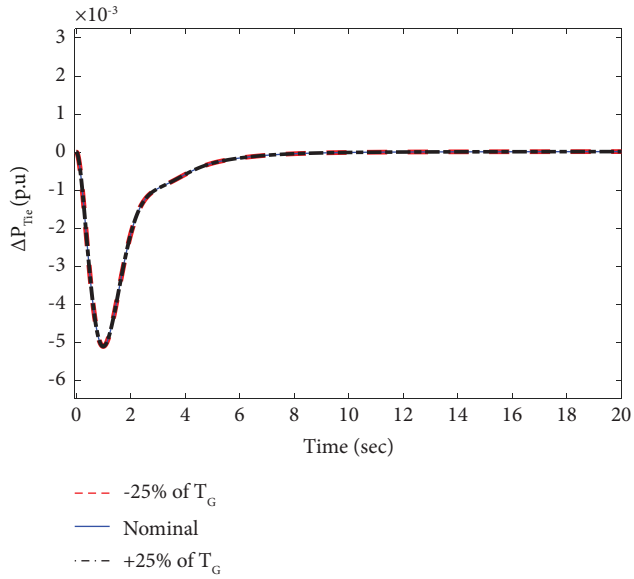

(c)

Figure 13: Dynamic performance with variation T_G (a) ΔF_1, (b) ΔF_2, and (c) ΔP_{Tie}.

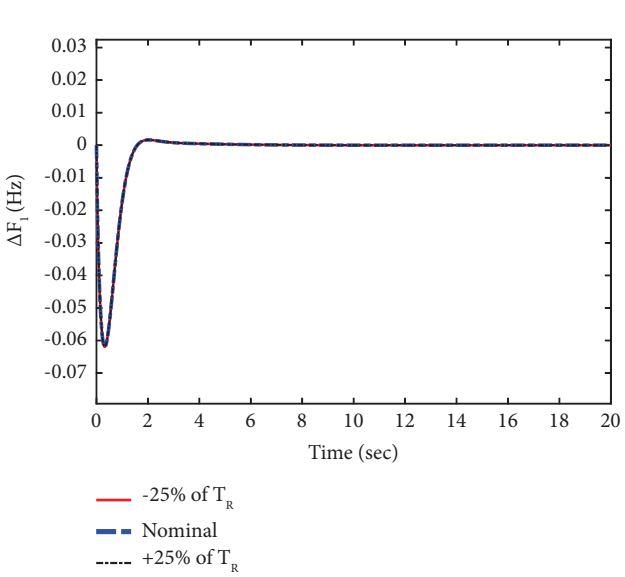

(a)

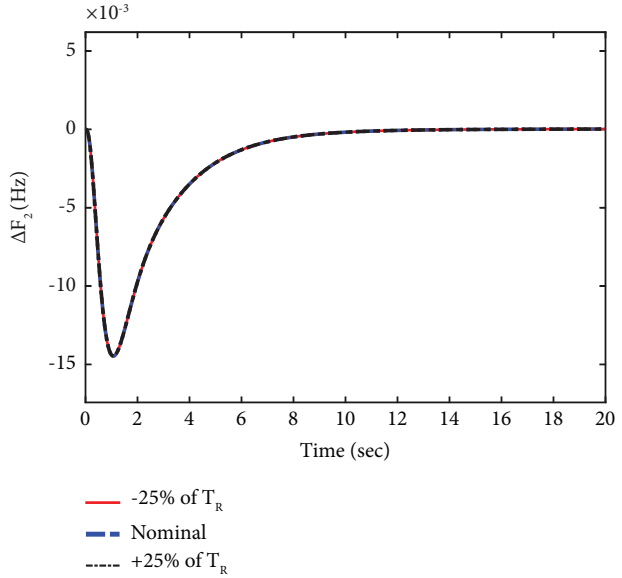

(b)

Figure 14: Continued.

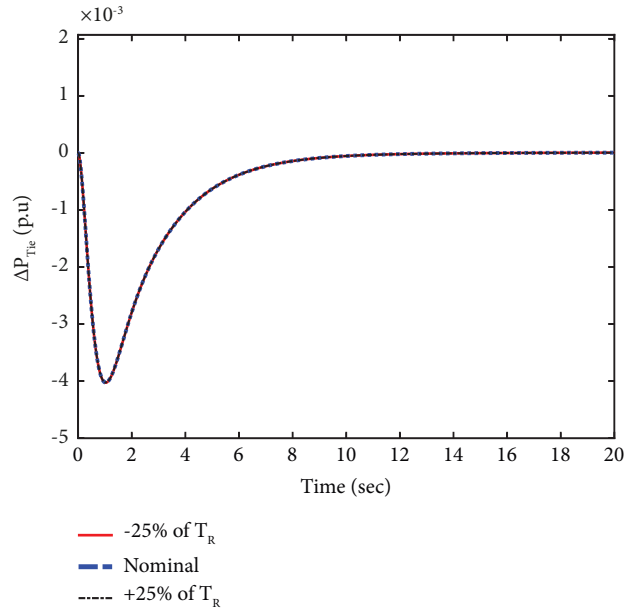

(c)

Figure 14: Dynamic performance with variation T_R (a) ΔF_1, (b) ΔF_2, and (c) ΔP_{Tie}.

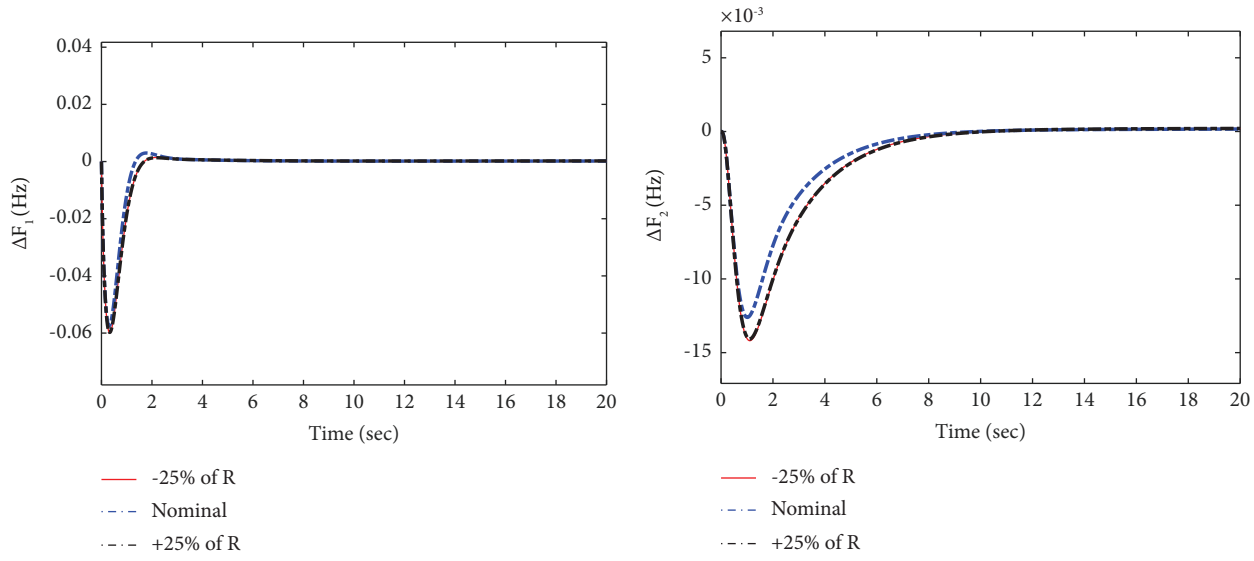

(a) (b)

Figure 15: Continued.

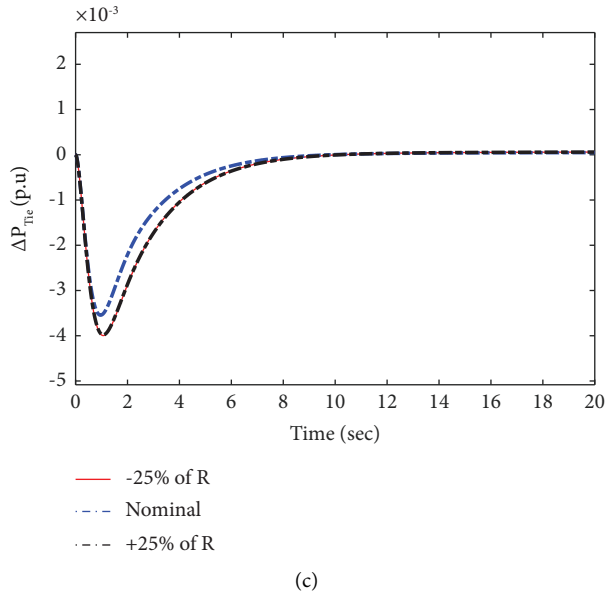

(c)

Figure 15: Dynamic performance with variation R (a) ΔF_1, (b) ΔF_2, and (c) ΔP_{Tie}.

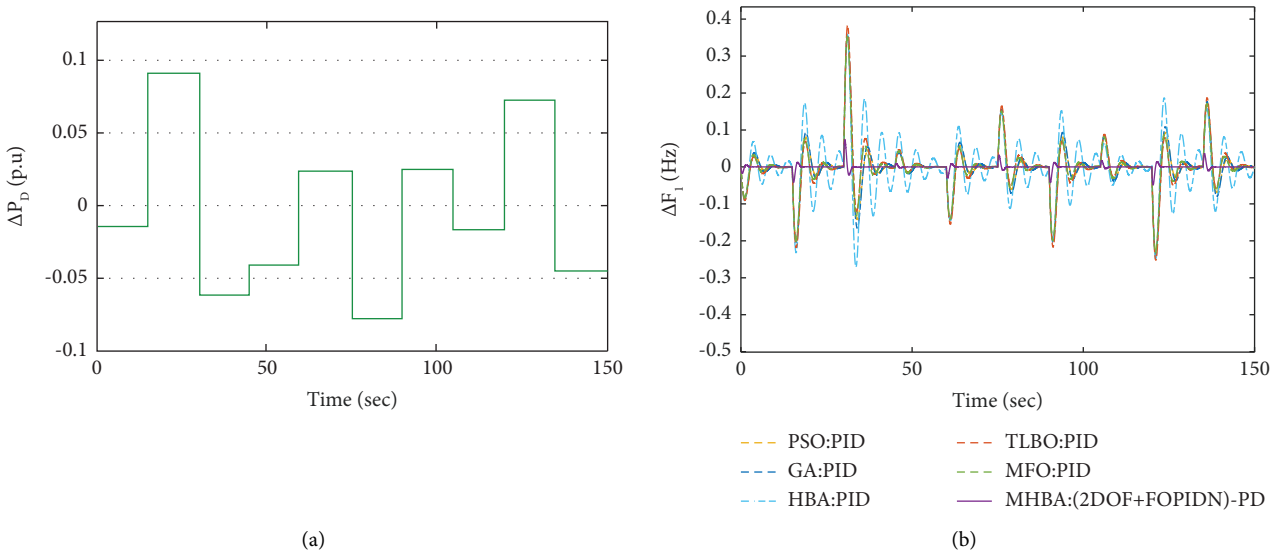

(a) (b)

Figure 16: Continued.

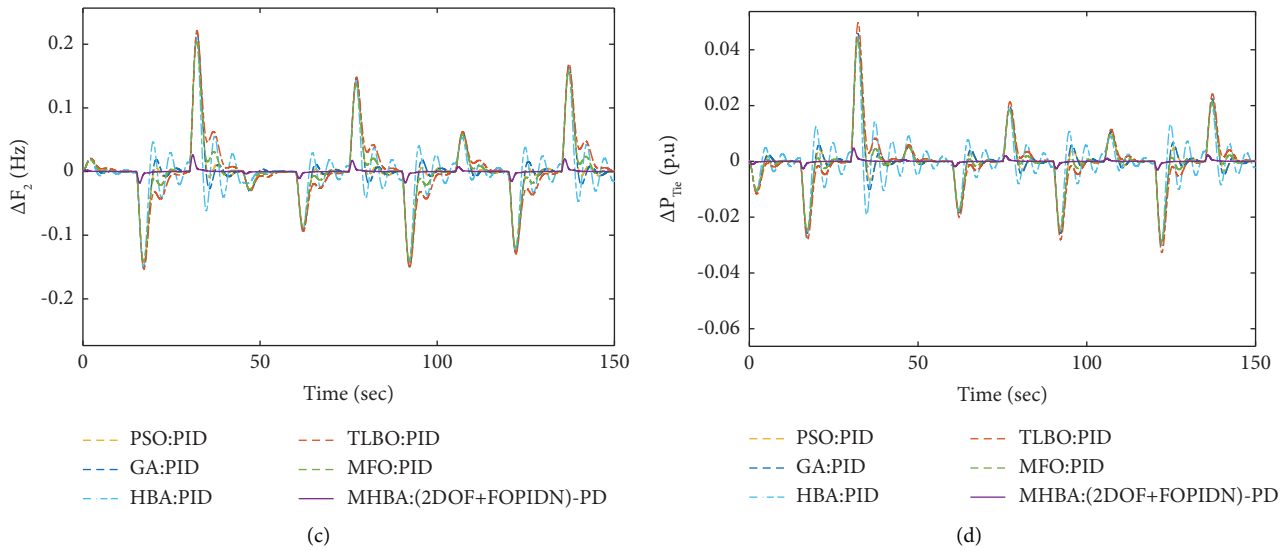

Figure 16: Dynamic response of the system under and random step load disturbance (a) RSL changes pattern, (b) ΔF_1, (c) ΔF_2, and (d)ΔP_{Tie}.

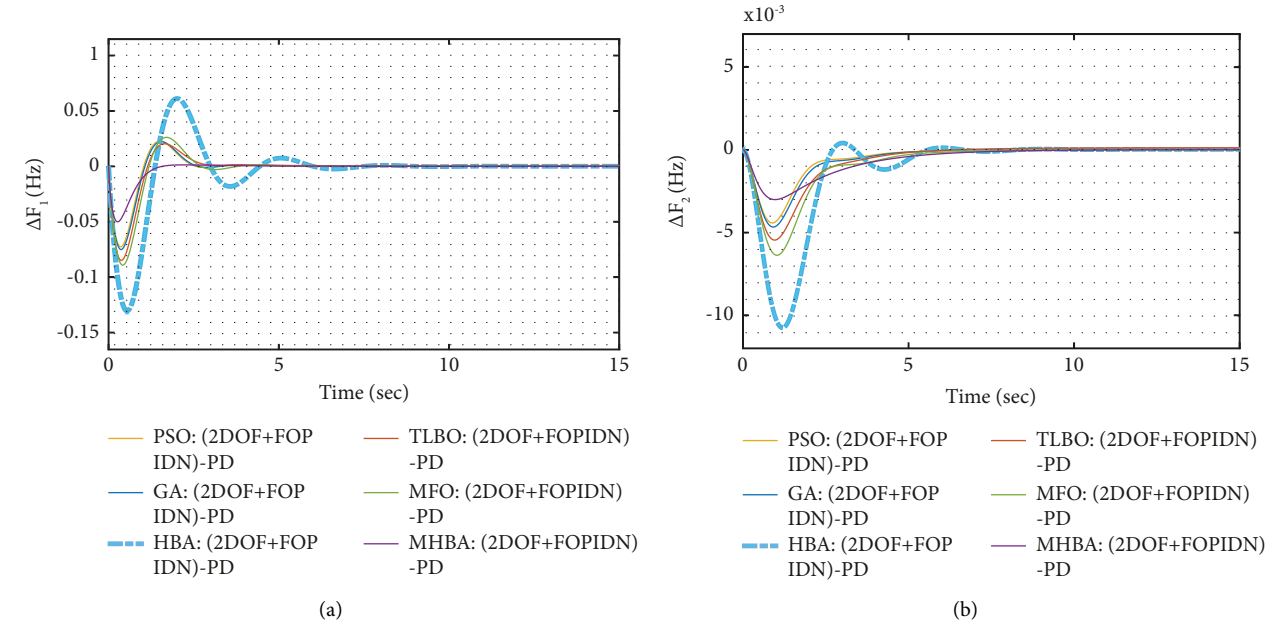

Figure 17: Continued.

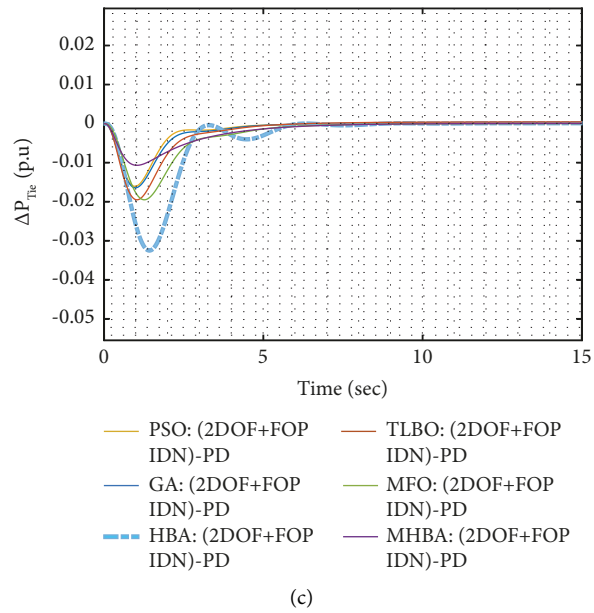

(c)

Figure 17: Dynamic performance of the IPS model (a) ΔF_1, (b) ΔF_2, and (c) ΔP_{Tie}.

Table 7: Dynamic response of the IPS with (2DOF + FOPIDN)-PD controllers.

Controllers	ITSE	Settling time (s) (T_s)			Undershoot (U_{sh})		
		ΔF_1	ΔF_2	ΔP_{tie}	ΔF_1	ΔF_2	ΔP_{tie}
GA	0.0011	2.4937	7.1885	7.0623	0.0217	0.0303	0.0133
TLBO	0.0019	4.7830	4.8845	4.9169	0.0134	0.0144	0.0339
MFO	0.0017	2.9584	7.5915	8.4744	0.0180	0.0303	0.0303
PSO	0.0009	2.5076	6.5486	6.5246	0.0528	0.0119	0.0303
HBA	0.0075	2.9637	5.4543	6.2800	0.0745	0.0175	0.0242
MHBA	0.0004	2.4799	8.1731	8.1733	0.0032	0.0013	0.0125

the resiliency of the proposed approach in scenarios 1 and 2 as well as with only the IPFC.

5.3. Sensitivity Study. A system's ability to continue to function as intended when its variables fluctuate within a specified tolerance range is known as its robustness [73]. For the purpose of evaluating the robustness of the MHBA-tuned (2DOF + FOPIDN)-PD, there have been a number of sensitivity analyses performed, including wide discrepancies of system parameters (T_G, T_R, and R) are in this context regulated from their nominal values in the range of ±25%. The respective output values of the settling time and undershoot for both areas are presented in Table 6. As indicated in Table 6 and Figures 13(a)–13(c), a wide discrepancy of the system parameter (T_g) results in a minor change in the corresponding undershoot and response settling time of the IPS system. In a similar vein, changes in system parameter, T_R, yielded a similar response as in Table 6 and Figures 14(a)–14(c), which revealed little or no change in the dynamic response of the suggested control method. Moreover, variations in system parameter, R, are presented in Figures 15(a)–15(c). Little disparities are experienced in Table 6 and Figures 15(a)–15(c). Analyzing Table 6, it is evident that a wide variety of system parameters results in small changes in response settling times and undershoots. Therefore, it is obvious that the performance of the proposed MHBA-tuned (2DOF + FOPIDN)-PD controller is not affected by an extensive variation of the system parameters, which points to its adequacy. The potency of the proposed controller is reiterated under this sensitivity test. Hence, the proposed control method offers a control scheme with sufficient reliability and robustness.

5.4. Random Load Disturbance. Figures 16(a)–16(d) present the system's robustness to random step load perturbation in all areas, providing additional insight into the system's robustness. The random step load (RSL) changes pattern is described in Figure 16(a). The proposed method performed better than any other, as shown in Figure 16(b) by examining the nature of its curve. Furthermore, a comparable response is seen in area 2 with a lesser perturbation and reduced undershoots as illustrated in Figure 16(c). The steadiness of the proposed approach for the tie-line power deviation can also be appreciated in the pattern of its curve by exhibiting the least deviant curve compared to alternative approaches as shown in Figure 16(d). Again, the

results validated the suggested approach's resilience under a variety of situations, including random load step perturbation this time.

5.5. Dynamic Response of the IPS with (2DOF + FOPIDN)-PD. This subsection examined the application of PSO, GA, HBA, TLBO, MFO, HBA, and MHBA for optimizing the (2DOF + FOPIDN)-PD controller. It can be observed from Figures 17(a)–17(c) that the proposed MHBA curve delivered the best curve with lesser damping and the least settling time. The same pattern is obtained for ΔF_1 in area 1, ΔF_2 in area 2, and the ΔP_{Tie}. In addition, the MHBA-based (2DOF + FOPIDN)-PD delivered the best value for the ITSE (0.0004125) compared with other methods. In terms of the settling time, the MHBA-based (2DOF + FOPIDN)-PD exhibited the best performance in area 1 compared to other methods. Nevertheless, the TLBO-based (2DOF + FOPIDN)-PD delivered a better performance for the setting time of area 2 and the tie-line. Compared with other methods, the MHBA-based (2DOF + FOPIDN)-PD outperformed other methods regarding the undershoot. This is evident in the figures and Table 7. The overall performance of the MHBA-based (2DOF + FOPIDN)-PD showed an improved performance compared to other methods.

6. Conclusion

This work presented the application of a modified honey badger algorithm (HBA) to control the frequency and tie-line power deviations in unequal multiarea interconnected power systems with conventional and renewable energy sources (RES). Moreover, for a realistic design, the performance of the control scheme was assessed by using an integral time square error index (ITSE), while simultaneously including redox flow batteries (RFBs) and interline power flow controllers (IPFCs) into the IPS architecture. An innovative cascaded two-degree-of-freedom fractional-order PID controller structure, coupled with a proportional derivative (FOPIDN)-PD controller, has been developed for the LFC power system. A recent optimization algorithm based on the modelling behaviour of the honey badger known as the honey badger algorithm (HBA) was applied to tune the parameters of the cascaded (2DOF + FOPIDN)-PD controllers. To improve the exploratory abilities of the standard HBA, the Lévy flight and a modified inertia weight were incorporated so the improved algorithm could successfully traverse complex search spaces without getting stuck at local optima (LO). To begin with, three different scenarios were first used to evaluate the performance of the proposed control scheme. We evaluated the efficiency of the proposed algorithm by comparing its dynamic response to some recently published and widely used metaheuristic algorithms. The proposed solution delivered the highest performance with the minimum ITSE, settle time, and undershoot values. This study demonstrates that the developed control scheme aggregate performance can enable high reliability over a wide range of load condition scenarios, sensitivity tests, and random load perturbations, which are essential to confirm both the efficiency and the reliability of the control technique.

There may be scope for further investigation of incorporating fuzzy logic tuning rules into the proposed control scheme. In addition, other contemporary optimization algorithms might also be used to improve the suggested controller's settings. Lastly, further studies could be carried out by performing a hardware-in-the-loop simulation.

Abbreviations

LFC: Load frequency control
HBA: Honey badger algorithm
IPS: Interconnected power system
RES: Renewable energy source
PS: Power system
SC: Soft computing
BFOA: Bacterial foraging optimization algorithm
DE: Differential evolution
QOHS: quasi-oppositional harmony search
GDB: Governor dead band
GRC: Generation rate constant
NN: Neural networks
ANFIS: Adaptive neuro-fuzzy interface systems
ICA: Imperialist competitive algorithm
PID: Proportional integral derivative
PI: Proportional integral
PD: Proportional derivative
ITAE: Integral time absolute error
ITSE: Integral time square error
2DOF: 2-Degree Freedom
FOPID: Fractional order proportional-integral derivative
LF: Lévy flight
MSIPS: Multi-source interconnected power system
FOC: Fractional order calculus
FACTS: Flexible alternating current transmission system
LO: Local optima.
RLD: Random load disturbance.

Appendix

Thermal and hydropower plant data are from Saadat [74] and Daraz et al. [31]. Wind and diesel power plants are from Barisal and Mishra [75], and Das et al. [76].

The nominal parameters of the system model are as follows: $P_R = 2000MW, P_L = 1000MW, f = 60Hz$, $T_{G1} = 0.2$ s, $T_{G2} = 0.3$ s, $T_{T1} = 0.5$ s, $T_{T2} = 0.5$ s, $K_1 = 0.30$, $T_R = 10$ s, $T_{RH} = 28.70$ s, $T_{GH} = 0.2$ s, $T_R = 10$ s, $T_w = 1$ s, $K_{pc} = 0.8$, $K_T = 0.5747$, $K_{\text{Diesel}} = 16.5, K_D = 0.2873$, $K_W = 0.138$, $T_{wd1} = 0.041, T_{wd2} = 0.6$, $K_{wd1} = 1.25, K_{wd2} = 1.3, D_1 = 0.6$, $D_2 = 0.9, H_1 = 5, H_2 = 5, K_{DG} = 16.5, T_D = 0.025, a_{12} = -1$, $K_p = 1/D$, $T_p = 2H/Df, P_{12} = 2$ p.u, $R_{T1} = R_{H1} = R_{G1} = 0.05$ Hz/pu, $R_{T2} = R_{H2} = R_{G2} = 0.0625$; boiler dynamics: Sahu, Prusty, and Panda [51]: $K_2 = 0.85$, $K_3 = 0.095$, $K_4 = 0.92, C_{BD} = 200, K_{BD} = 0.03, T_{BD} = 26$ s, $T_{RBD} = 69$ s, $T_{DM} = 0$, $T_{FD} = 10$ s.

RFBS and IPFC parameters are as follows: Naga and Sambasiva [77]: $K_{RFBs} = 1, T_{RFBs} = 0.9$, $K_1 = 0.2, K_2 = -0.1$, $T_{IPFC} = 0.0450$.

Data Availability

The data used to support the findings of this study are available from the corresponding author upon request.

Conflicts of Interest

The authors declare no conflicts of interest.

Acknowledgments

This work was supported in part by the South African National Research Foundation under Grant nos. 137951, 141951, and 132797 and the South African National Research Foundation Incentive under Grant 132159.

References

[1] O. I. Elgerd, *Electric Energy Systems Theory - an Introduction*, McGraw-Hill, New York, NY, USA, Second ed edition, 2000.

[2] P. Kundur, N. J. Balu, and M. G. Lauby, *Power System Stability And Control*, vol. 7, McGraw-Hill, New York, NY, USA, 1994.

[3] H. Gozde, M. Cengiz Taplamacioglu, and I. Kocaarslan, "Comparative performance analysis of Artificial Bee Colony algorithm in automatic generation control for interconnected reheat thermal power system," *International Journal of Electrical Power & Energy Systems*, vol. 42, no. 1, pp. 167–178, 2012.

[4] S. P. Singh, T. Prakash, and V. P. Singh, "Coordinated tuning of controller-parameters using symbiotic organisms search algorithm for frequency regulation of multi-area wind integrated power system," *Engineering Science and Technology, an International Journal*, vol. 23, no. 1, pp. 240–252, 2020.

[5] J. R. Nayak, B. Shaw, and B. K. Sahu, "Implementation of hybrid SSA-SA based three-degree-of-freedom fractional-order PID controller for AGC of a two-area power system integrated with small hydro plants," *IET Generation, Transmission & Distribution*, vol. 14, no. 13, pp. 2430–2440, 2020.

[6] S. Oladipo, Y. Sun, and Z. Wang, "An enhanced flower pollinated algorithm with a modified fluctuation rate for global optimisation and load frequency control system," *IET Renewable Power Generation*, vol. 16, no. 6, pp. 1220–1245, 2022.

[7] Y. Arya, "A new optimized fuzzy FOPI-FOPD controller for automatic generation control of electric power systems," *Journal of the Franklin Institute*, vol. 356, no. 11, pp. 5611–5629, 2019.

[8] E. Çelik, N. Öztürk, Y. Arya, and C. Ocak, "(1 + PD)-PID cascade controller design for performance betterment of load frequency control in diverse electric power systems," *Neural Computing & Applications*, vol. 33, no. 22, pp. 15433–15456, 2021.

[9] S. Panda and N. K. Yegireddy, "Automatic generation control of multi-area power system using multi-objective non-dominated sorting genetic algorithm-II," *International Journal of Electrical Power & Energy Systems*, vol. 53, no. 1, pp. 54–63, 2013.

[10] L. C. Saikia, J. Nanda, and S. Mishra, "Performance comparison of several classical controllers in AGC for multi-area interconnected thermal system," *International Journal of Electrical Power & Energy Systems*, vol. 33, no. 3, pp. 394–401, 2011.

[11] M. H. Kazemi, M. Karrari, and M. B. Menhaj, "Decentralized robust adaptive-output feedback controller for power system load frequency control," *Electrical Engineering*, vol. 84, no. 2, pp. 75–83, 2002.

[12] K. P. Singh Parmar, S. Majhi, and D. P. Kothari, "Load Frequency Control of a Realistic Power System with Multi-Source Power Generation," *International Journal of Electrical Power \& Energy System*, vol. 42, 2012.

[13] H. Bevrani and T. Hiyama, "Robust decentralised PI based LFC design for time delay power systems," *Energy Conversion and Management*, vol. 49, no. 2, pp. 193–204, 2008.

[14] A. D. Rosaline and U. Somarajan, "Structured H-Infinity controller for an uncertain deregulated power system," *IEEE Transactions on Industry Applications*, vol. 55, no. 1, pp. 892–906, 2019.

[15] M. Azzam, "Robust automatic generation control," *Energy Conversion and Management*, vol. 40, no. 13, pp. 1413–1421, 1999.

[16] W. Tan, "Unified tuning of PID load frequency controller for power systems via IMC," *IEEE Transactions on Power Systems*, vol. 25, no. 1, pp. 341–350, 2010.

[17] D. H. Tungadio and Y. Sun, "Load frequency controllers considering renewable energy integration in power system," *Energy Reports*, Elsevier, vol. 5, pp. 436–453, 2019.

[18] S. Oladipo, Y. Sun, and Z. Wang, "Optimization of PID and FOPID controllers with new generation metaheuristic algorithms for controlling AVR system: concise Survey," in *Proceedings of the 2020 12th International Conference on Computational Intelligence and Communication Networks (CICN)*, pp. 280–286, Bhimtal, India, September 2020.

[19] A. El-Gammal, "Particle swarm optimization-based BLDC motor speed controller with response speed consideration," in *Proceedings of the 2017 International Seminar on Intelligent Technology and Its Application: Strengthening the Link Between University Research and Industry to Support ASEAN Energy Sector*, pp. 193–198, ISITIA 2017, Surabaya, Indonesia, August 2017.

[20] S. Saxena and Y. V. Hote, "PI controller based load frequency control approach for single-area power system having communication delay," *IFAC-PapersOnLine*, vol. 51, no. 4, pp. 622–626, 2018.

[21] E. S. Ali and S. M. Abd-Elazim, "Bacteria foraging optimization algorithm based load frequency controller for interconnected power system," *International Journal of Electrical Power & Energy Systems*, vol. 33, no. 3, pp. 633–638, 2011.

[22] B. Mohanty, S. Panda, and P. K. Hota, "Controller parameters tuning of differential evolution algorithm and its application to load frequency control of multi-source power system," *International Journal of Electrical Power & Energy Systems*, vol. 54, pp. 77–85, 2014.

[23] C. K. Shiva and V. Mukherjee, "Design and analysis of multi-source multi-area deregulated power system for automatic generation control using quasi-oppositional harmony search algorithm," *International Journal of Electrical Power & Energy Systems*, vol. 80, pp. 382–395, 2016.

[24] D. Guha, P. K. Roy, and S. Banerjee, "Load frequency control of large scale power system using quasi-oppositional grey wolf optimization algorithm," *Engineering Science and Technology, an International Journal*, vol. 19, no. 4, pp. 1693–1713, 2016.

[25] H. Shabani, B. Vahidi, and M. Ebrahimpour, "A robust PID controller based on imperialist competitive algorithm for load-frequency control of power systems," *ISA Transactions*, vol. 52, no. 1, pp. 88–95, 2013.

[26] C. S. Ali Nandar, "Robust PI control of smart controllable load for frequency stabilization of microgrid power system," *Renewable Energy*, vol. 56, pp. 16–23, 2013.

[27] D. Guha, P. K. Roy, and S. Banerjee, "Study of differential search algorithm based automatic generation control of an interconnected thermal-thermal system with governor deadband," *Applied Soft Computing*, vol. 52, pp. 160–175, 2017.

[28] D. Guha, P. K. Roy, and S. Banerjee, "Load frequency control of interconnected power system using grey wolf optimization," *Swarm and Evolutionary Computation*, vol. 27, pp. 97–115, 2016.

[29] R. K. Sahu, S. Panda, U. K. Rout, and D. K. Sahoo, "Teaching learning based optimization algorithm for automatic generation control of power system using 2-DOF PID controller," *International Journal of Electrical Power & Energy Systems*, vol. 77, pp. 287–301, 2016.

[30] N. C. Patel, M. K. Debnath, B. K. Sahu, and P. Das, "2DOF-PID controller-based load frequency control of linear/nonlinear unified power system," *Advances in Intelligent Systems and Computing*, vol. 846, pp. 227–236, 2019.

[31] A. Daraz, S. A. Malik, I. U. Haq, K. B. Khan, G. F. Laghari, and F. Zafar, "Modified PID controller for automatic generation control of multi-source interconnected power system using fitness dependent optimizer algorithm," *PLoS One*, vol. 15, no. 11, Article ID e0242428, 2020.

[32] N. C. Patel, B. K. Sahu, D. P. Bagarty, P. Das, and M. K. Debnath, "A novel application of ALO-based fractional order fuzzy PID controller for AGC of power system with diverse sources of generation," *International Journal of Electrical Engineering Education*, vol. 58, no. 2, pp. 465–487, 2019.

[33] P. Sharma, A. Prakash, R. Shankar, and S. K. Parida, "A novel hybrid salp swarm differential evolution algorithm based 2DOF tilted-integral-derivative controller for restructured AGC," *Electric Power Components and Systems*, vol. 47, no. 19–20, pp. 1775–1790, 2019.

[34] M. Sharma, S. Prakash, S. Saxena, and S. Dhundhara, "Optimal fractional-order tilted-integral-derivative controller for frequency stabilization in hybrid power system using salp swarm algorithm," *Electric Power Components and Systems*, vol. 48, no. 18, pp. 1912–1931, 2021.

[35] S. Oladipo, Y. Sun, and Z. Wang, "Application of a new fusion of flower pollinated with pathfinder algorithm for AGC of multi-source interconnected power system," *IEEE Access*, vol. 9, pp. 94149–94168, 2021.

[36] S. Debbarma and A. Dutta, "Utilizing electric vehicles for LFC in restructured power systems using fractional order controller," *IEEE Transactions on Smart Grid*, vol. 8, no. 6, pp. 2554–2564, 2017.

[37] M. Farahani, S. Ganjefar, and M. Alizadeh, "PID controller adjustment using chaotic optimisation algorithm for multi-area load frequency control," *IET Control Theory & Applications*, vol. 6, no. 13, pp. 1984–1992, 2012.

[38] K. Chandran, R. Murugesan, S. Gurusamy et al., "Modified cascade controller design for unstable processes with large dead time," *IEEE Access*, vol. 8, pp. 157022–157036, 2020.

[39] H. A. Suthar and J. J. Gadit, "Two degree of freedom controller optimization using GA for shell and tube heat exchanger," in *Proceedings of the 2017 11th International Conference on Intelligent Systems and Control (ISCO)*, pp. 1–7, Coimbatore, India, February 2017.

[40] B. K. Sahu, S. Panda, P. K. Mohanty, and N. Mishra, "Robust analysis and design of PID controlled AVR system using Pattern Search algorithm," in *Proceedings of the PEDES 2012 - IEEE International Conference on Power Electronics, Drives and Energy Systems*, pp. 1–6, Bengaluru, India, December 2012.

[41] S. Arora, H. Singh, M. Sharma, S. Sharma, and P. Anand, "A new hybrid algorithm based on grey wolf optimization and crow search algorithm for unconstrained function optimization and feature selection," *IEEE Access*, vol. 7, pp. 26343–26361, 2019.

[42] F. A. Hashim, E. H. Houssein, K. Hussain, M. S. Mabrouk, and W. Al-Atabany, "Honey Badger Algorithm: new metaheuristic algorithm for solving optimization problems," *Mathematics and Computers in Simulation*, vol. 192, pp. 84–110, 2022.

[43] Z. Li, Y. Zhou, S. Zhang, and J. Song, "Lévy-flight moth-flame algorithm for function optimization and engineering design problems," *Mathematical Problems in Engineering*, vol. 2016, pp. 1–22, Article ID 1423930, 2016.

[44] Y. Ling, Y. Zhou, and Q. Luo, "Lévy flight trajectory-based whale optimization algorithm for global optimization," *IEEE Access*, vol. 5, pp. 6168–6186, 2017.

[45] S. Kohli, M. Kaushik, K. Chugh, and A. C. Pandey, "Levy inspired enhanced grey wolf optimizer," in *Proceedings of the IEEE International Conference Image Information Processing*, pp. 338–342, Shimla, India, November 2019.

[46] S. Amirsadri, S. J. Mousavirad, and H. Ebrahimpour-Komleh, "A Levy flight-based grey wolf optimizer combined with back-propagation algorithm for neural network training," *Neural Computing & Applications*, vol. 30, no. 12, pp. 3707–3720, 2018.

[47] B. Mohanty, S. Panda, and P. K. Hota, "Differential evolution algorithm based automatic generation control for interconnected power systems with non-linearity," *Alexandria Engineering Journal*, vol. 53, no. 3, pp. 537–552, 2014.

[48] D. Guha, P. K. Roy, and S. Banerjee, "Symbiotic organism search algorithm applied to load frequency control of multi-area power system," *Energy Syst*, vol. 9, no. 2, pp. 439–468, 2018.

[49] R. K. Sahu, T. S. Gorripotu, and S. Panda, "Automatic generation control of multi-area power systems with diverse energy sources using Teaching Learning Based Optimization algorithm," *Engineering Science and Technology, an International Journal*, vol. 19, no. 1, pp. 113–134, 2016.

[50] C. H. N. S. Kalyan and G. S. Rao, "Impact of communication time delays on combined LFC and AVR of a multi-area hybrid system with IPFC-RFBs coordinated control strategy," *Prot. Control Mod. Power Syst.*vol. 6, no. 1, p. 7, 2021.

[51] P. C. Sahu, R. C. Prusty, and S. Panda, "Approaching hybridized GWO-SCA based type-II fuzzy controller in AGC of diverse energy source multi area power system," *Journal of King Saud University - Engineering Sciences*, vol. 32, no. 3, pp. 186–197, 2020.

[52] R. E. Gutiérrez, J. M. Rosário, and J. Tenreiro MacHado, "Fractional order calculus: basic concepts and engineering applications," *Mathematical Problems in Engineering*, vol. 2010, pp. 1–19, Article ID 375858, 2010.

[53] M. Al-Dhaifallah, N. Kanagaraj, and K. S. Nisar, "Fuzzy fractional-order PID controller for fractional model of pneumatic pressure system," *Mathematical Problems in Engineering*, vol. 2018, pp. 1–9, Article ID 5478781, 2018.

[54] J. Bhookya and R. K. Jatoth, "Optimal FOPID/PID controller parameters tuning for the AVR system based on sine–cosine-algorithm," *Evolutionary Intelligence*, vol. 12, no. 4, pp. 725–733, 2019.

[55] S. Das and S. Panda, *An Optimized Fractional Order cascade Controller for Frequency Regulation of Power System with Renewable Energies and Electric Vehicles*, Springer, Heidelberg, Germany, pp. 1–25, 2021.

[56] A. Oustaloup, F. Levron, B. Mathieu, and F. M. Nanot, "Frequency-band complex noninteger differentiator: characterization and synthesis," *IEEE Transactions on Circuits and Systems I: Fundamental Theory and Applications*, vol. 47, no. 1, pp. 25–39, 2000.

[57] I. Podlubny, "Fractional-order systems and PI/sup/spl lambda//D/sup/spl mu//-controllers," *IEEE Transactions on Automatic Control*, vol. 44, no. 1, pp. 208–214, 1999.

[58] M. A. Johnson and H. Mohammad, *New Identification and Design Methods*, Springer-Verlag, London, 2010.

[59] Y. K Soni and R Bhatt, "Simulated Annealing optimized PID controller design using ISE, IAE, IATE and MSE error criteria," *Int. J. Adv. Res. Comput. Eng. Technol.*vol. 2, pp. 1323–2337, 2013.

[60] H. Zhang and J. Wang, "Combined feedback-feedforward tracking control for networked control systems with probabilistic delays," *Journal of the Franklin Institute*, vol. 351, no. 6, pp. 3477–3489, 2014.

[61] D. J. Kapner, T. S. Cook, E. G. Adelberger et al., "Tests of the gravitational inverse-square law below the dark-energy length scale," *Physical Review Letters*, vol. 98, no. 2, p. 021101, 021101,.

[62] H. Hakli and H. Uğuz, "A novel particle swarm optimization algorithm with Levy flight," *Applied Soft Computing*, vol. 23, pp. 333–345, 2014.

[63] A. M. Reynolds and M. A. Frye, "Free-flight odor tracking in Drosophila is consistent with an optimal intermittent scale-free search," *PLoS One*, vol. 2, no. 4, p. e354, 2007.

[64] M. Gutowski, "Levy flights as an underlying mechanism for global optimization algorithms," in *Evolutionary Algorithms and Global Optimization*, pp. 1–8, 2001.

[65] I. Pavlyukevich, "Levy flights, non-local search and simulated annealing," *Journal of Computational Physics*, vol. 226, no. 2, pp. 1830–1844, 2007.

[66] X. S. Yang, Z. Cui, R. Xiao, A. H. Gandomi, and M. Karamanoglu, *Swarm Intelligence and Bio-Inspired Computation*, Elsevier, Hendon, 2013.

[67] S. Khan, M. Kamran, O. U. Rehman, L. Liu, and S. Yang, "A modified PSO algorithm with dynamic parameters for solving complex engineering design problem," *International Journal of Computer Mathematics*, vol. 95, no. 11, pp. 2308–2329, 2017.

[68] S. Oladipo, Y. Sun, and Z. Wang, "Optimization of FOPID controller with hybrid particle swarm and grey wolf optimization for AVR system," in *Proceedings of the 2020 12th International Conference on Computational Intelligence and Communication Networks (CICN)*, pp. 273–279, Bhimtal, India, September 2020.

[69] X. S. Yang and S. Deb, "Cuckoo search via Lévy flights," in *Proceedings of the 2009 World Congress on Nature and Biologically Inspired Computing, NABIC 2009 - Proceedings*, pp. 210–214, Coimbatore, India, December 2009.

[70] A. A. Al-Temeemy, J. W. Spencer, and J. F. Ralph, "Levy flights for improved Ladar scanning," in *Proceedings of the 2010 2010 IEEE International Conference on Imaging Systems and Techniques*, pp. 225–228, Thessaloniki, Greece, July 2010.

[71] R. N. Mantegna, "Fast, accurate algorithm for numerical simulation of Lévy stable stochastic processes," *Physical Review E - Statistical Physics, Plasmas, Fluids, and Related Interdisciplinary Topics*, vol. 49, no. 5, pp. 4677–4683, 1994.

[72] A. Tepljakov, E. Petlenkov, and J. Belikov, "Fomcon a MATLAB toolbox for fractional-order system identification and control," *Int. J. Microelectron. Comput. Sci.*vol. 2, no. 2, pp. 51–62, 2011.

[73] R. K. Sahu, S. Panda, and S. Padhan, "Optimal gravitational search algorithm for automatic generation control of interconnected power systems," *Ain Shams Engineering Journal*, vol. 5, no. 3, pp. 721–733, Sep. 2014.

[74] H. Saadat, *Power System Analysis*, McGraw-Hill, New York, NY, USA, 1999.

[75] A. K. Barisal and S. Mishra, "Improved PSO based automatic generation control of multi-source nonlinear power systems interconnected by AC/DC links," *Cogent Engineering*, vol. 5, no. 1, Article ID 1422228, 2018.

[76] D. Das, S. K. Aditya, and D. P. Kothari, "Dynamics of diesel and wind turbine generators on an isolated power system," *International Journal of Electrical Power & Energy Systems*, vol. 21, no. 3, pp. 183–189, 1999.

[77] C. H. N. S. Kalyan and G. S. Rao, "Impact of communication time delays on combined LFC and AVR of a multi-area hybrid system with IPFC-RFBs coordinated control strategy," *Prot. Control Mod. Power Syst.*vol. 6, no. 1, pp. 7–20, 2021.